FZR-422

Wissenschaftlich-Technische Berichte
FZR-422 März 2005 ISSN 1437-322X

Henry Moll, Mohamed Merroun,
Thorsten Stumpf, André Roßberg,
Gerhard Geipel, Sonja Selenska-Pobell
Gert Bernhard

Interaction of Actinides with the Predominant Indigenous Bacteria in Äspö Aquifer

Interactions of Selected Actinides U(VI), Cm(III), Np(V) and Pu(VI) with *Desulfovibrio äspöensis*

Forschungszentrum
Rossendorf

Wissenschaftlich-Technische Berichte
FZR-422
März 2005

Henry Moll, Mohamed Merroun, Thorsten Stumpf,
André Roßberg, Gerhard Geipel,
Sonja Selenska-Pobell, Gert Bernhard

Interaction of Actinides with the Predominant Indigenous Bacteria in Äspö Aquifer

Interactions of Selected Actinides U(VI),
Cm(III), Np(V) and Pu(VI) with
Desulfovibrio äspöensis

Forschungszentrum
Rossendorf

Abstract
Sulfate-reducing bacteria (SRB) frequently occur in the deep granitic rock aquifers at the Äspö Hard Rock Laboratory (Äspö HRL), Sweden. The new SRB strain *Desulfovibrio äspöensis* could be isolated. The objective of this project was to explore the basic interaction mechanisms of uranium, curium, neptunium and plutonium with cells of *D. äspöensis* DSM 10631^T.
The cells of *D. äspöensis* were successfully cultivated under anaerobic conditions as well in an optimized bicarbonate-buffered mineral medium as on solid medium at 22 °C. To study the interaction of *D. äspöensis* with the actinides, the cells were grown to the mid-exponential phase (four days). The collected biomass was usually 1.0±0.2 $g_{dry\ weight}$/L. The purity of the used bacterial cultures was verified using microscopic techniques and by applying the Amplified Ribosomal DNA Restriction Enzyme Analysis (ARDREA).
The interaction experiments with the actinides showed that the cells are able to remove all four actinides from the surrounding solution. The amount of removed actinide and the interaction mechanism varied among the different actinides.
The main U(VI) removal occurred after the first 24 h. The contact time, pH and $[U(VI)]_{initial}$ influence the U removal efficiency. The presence of uranium caused a damaging of the cell membranes. TEM revealed an accumulation of U inside the bacterial cell. *D. äspöensis* are able to form U(IV). A complex interaction mechanism takes place consisting of biosorption, bioreduction and bioaccumulation.
Neptunium interacts in a similar way. The experimental findings are indicating a stronger interaction with uranium compared to neptunium.
The results obtained with ^{242}Pu indicate the ability of the cells of *D. äspöensis* to accumulate and to reduce Pu(VI) from a solution containing Pu(VI) and Pu(IV)-polymers.
In the case of curium at a much lower metal concentration of $3x10^{-7}$ M, a pure biosorption of Cm(III) on the cell envelope forming an inner-sphere surface complex most likely with organic phosphate groups was detected.
To summarize, the strength of the interaction of *D. äspöensis* with the selected actinides at pH 5 and actinide concentrations ≥ 10 mg/L ([Cm] 0.07 mg/L) follows the pattern: Cm > U > Pu >> Np.

Zusammenfassung

Sulfat-reduzierende Bakterien (SRB) wurden im tiefen granitischen Aquifer-System des Äspö Hard Rock Laboratoriums (Äspö HRL), Schweden, nachgewiesen. Es gelang, einen neuen SRB Stamm: *Desulfovibrio äspöensis* zu isolieren. Ziel des Projektes war die Untersuchung grundlegender Prozesse der Wechselwirkung von Uran, Curium, Neptunium und Plutonium mit Zellen von *D. äspöensis* DSM 10631^T.
Der Stamm *D. äspöensis* konnte erfolgreich unter anaeroben Bedingungen bei 22 °C im optimierten bikarbonat-gepuffertem Flüssigmedium und auf festem Medium kultiviert werden. Für die Studien mit den Actiniden erfolgte die Kultivierung bis zur Mitte der exponentiellen Wachstumskurve (4 Tage). Die Biomassemenge lag in der Regel im Bereich von 1.0±0.2 $g_{Trockenmasse}$/l. Die Reinheit der Kulturen wurde mikroskopisch und mittels Amplified Ribosomal DNA Restriction Enzyme Analysis (ARDREA) sichergestellt. Es konnte gezeigt werden, dass die Zellen alle vier Actiniden aus der Angebotslösung entfernen. Die Menge an entferntem Actinid und die Art des Wechselwirkungs-mechanismusses variierten zwischen den unterschiedlichen Actiniden. Innerhalb der ersten 24 h wurde der Hauptanteil des U(VI) entfernt. Die Kontaktzeit, der pH-Wert und $[U(VI)]_{initial}$ beeinflussen stark die Effektivität der Urananbindung an die Biomasse. Die Anwesenheit des Urans bewirkt eine Schädigung des Membransystems der Zellen. TEM zeigte eine Akkumulation des U innerhalb der Zellen. *D. äspöensis* ist in der Lage U(IV) zu bilden. Ein komplexer Mechanismus findet statt, der aus Biosorption, Bioreduktion und Bioakkumulation besteht. Neptunium verhält sich ähnlich. Die Untersuchungen zeigten jedoch eine stärke Wechselwirkung von U(VI) mit den Zellen im Vergleich zum Np(V). Die Untersuchungen mit ^{242}Pu zeigten, daß die Zellen in der Lage sind aus einer Pu-Lösung die Pu(VI) und Pu(IV)-Polymere enthält, Pu(VI) zu binden und dieses schnell zu reduzieren. Im Falle von Cm(III) und bei deutlich niedrigeren Metallkonzentrationen von $3x10^{-7}$ M, dominiert die Biosorption unter Bildung eines inner-sphärischen Oberflächenkomplexes wahrscheinlich an organischen Phosphatgruppen der Zellwandstruktur.
Zusammenfassend ist festzustellen, dass bei pH 5 und Actinide-Konzentrationen ≥ 10 mg/l ([Cm] 0.07 mg/l) die Intensität der Wechselwirkung vom Cm zum Np abnimmt: Cm > U > Pu >> Np.

Content

1	**Introduction**	**1**
2	**Cultivation and characterization of the *Desulfovibrio äspöensis* biomass**	**2**
2.1	Optimization of the growing conditions in liquid medium	2
2.1.1	Growth curve of *D. äspöensis* in liquid medium	2
2.2	Growing on solid medium	3
2.3	Characterization of *D. äspöensis* cultures	4
2.3.1	Light Microscopy and Scanning Electron Microscopy (SEM)	4
2.3.2	Molecular analysis of *D. äspöensis* cultures	5
3	**Studies on the interaction of *Desulfovibrio äspöensis* cells with the selected actinides**	**6**
3.1	Interaction with uranium(VI)	6
3.1.1	Experimental	6
3.1.2	Uranium(VI) removal by the biomass	7
3.1.3	Toxicity of U(VI) towards *D. äspöensis* studied by flow cytometry and fluorescence microscopy	10
3.1.4	Speciation of U associated with the biomass investigated by means of XAFS Spectroscopy and LIPAS	12
3.1.5	Localization of the uranium associated with the biomass using TEM	16
3.1.6	Summary of the uranium results	18
3.2	Interaction with curium(III)	19
3.2.1	Experimental	19
3.2.2	Results and discussion	20
3.2.3	Interaction of Cm(III) with relevant model compounds	25
3.3	Interaction with neptunium(V)	29
3.3.1	Experimental	29
3.3.2	Results and discussion	30
3.4	Interaction with plutonium	33
3.4.1	Experimental	34
3.4.2	Results and discussion	37
4	**Summary and conclusions**	**51**
5	**References**	**54**
6	**Acknowledgement**	**59**

1 Introduction

The influence of microorganisms on migration processes of actinides has to be taken into account for the risk assessment of potential high level nuclear waste disposal sites. Therefore it is necessary to characterize the actinide-bacteria species formed and to elucidate the reaction mechanisms involved. Microbial activities can cause either dissolution and mobilization or immobilization of actinides by direct or indirect microbial actions in deep nuclear repositories and its environment, e.g., at the Äspö HRL. The Äspö (HRL) was established in Sweden in a granite rock formation for in-situ experiments with radionuclides. The aims of this facility are to examine which methods are most suitable for research in the bedrock, to develop and to demonstrate methods for deciding in what way a deep repository can be planned and constructed in accordance with the local characteristics of the bedrock, to increase scientific understanding of a deep repository's safety margins and to develop and demonstrate the technique that will be used during the disposal of spent nuclear fuel.
Investigations of the microbial diversity at the Äspö site were published by Pedersen et al. [1-3]. The total number of microorganisms measured at Äspö range from $1x10^3$ to $5x10^6$ cells ml^{-1}, whereas the number of sulfate-reducing bacteria (SRB) was between 10^1 to $2x10^4$ cells ml^{-1}. The analysis of the bacterial populations of SRB in the Äspö aquifer is very important. In addition to their ability to reduce many metals and actinides/radionuclides, they posses also a corrosive potential for the used copper canisters due to their sulfide production. Over the last years the interest increased in SRB and their interaction with actinides.
Our project is focused on the recovered SRB strain *D. äspöensis* which is indigenous at the Äspö site [4]. The aim of the presented work is to explore interaction processes of *D. äspöensis* with the actinides uranium, curium, neptunium, and plutonium. It is unknown in which way *D. äspöensis* cells are interacting with the selected actinides. To summarize, the main goals of the project are:

(i) Interaction of uranium, curium, neptunium and plutonium with *D. äspöensis* cells.
(ii) Quantification of actinides bonded on the microbes in dependence of the experimental parameters.
(iii) Spectroscopic characterization of the formed actinide complexes/compounds.

The obtained results should help to improve the scientific basis for the performance assessment and safety of nuclear waste repositories concerning the influence of microorganisms on actinide migration.

The scientific results of this project are described in detail in the following sections.

2 Cultivation and characterization of the *Desulfovibrio äspöensis* biomass

The basis for all following investigations is the successful and continuous cultivation and quality control of the *Desulfovibrio äspöensis* biomass.

2.1 Optimization of the growing conditions in liquid medium

The starting point of our investigations was a 10 ml active culture of the strain *Desulfovibrio äspöensis* DSM 10631^T obtained from the Deutsche Sammlung von Mikroorganismen und Zellkulturen GmbH (DSMZ, Braunschweig). The strain *D. äspöensis* was grown under anaerobic conditions in an optimized 250 ml bicarbonate-buffered mineral medium (DSMZ – Medium 721) containing resazurin as a redox indicator at 22 °C. The amount of ferrous chloride was stepwise reduced from $7.5x10^{-6}$ to $7.5x10^{-7}$ mol/L. The reason was to minimize the amount of inorganic sulfide associated with the biomass which could influence the results of the experiments with the actinides. The main components of the medium are 7 g/L of NaCl, 5 g/L of $NaHCO_3$, 3 g/L of Na_2SO_4, 2.5 g/L of sodium lactate, 1.5 g/L of $MgCl_2x6H_2O$, and 0.4 g/L of Na_2Sx9H_2O.

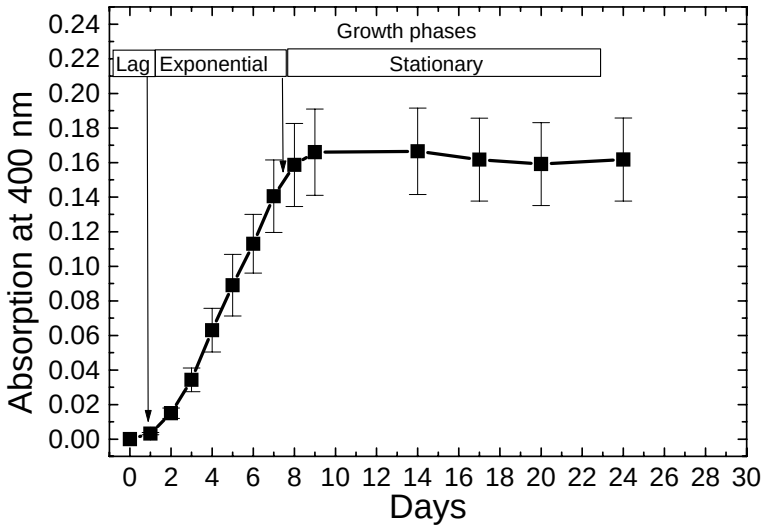

Fig. 2.1: Typical growth curve for *D. äspöensis* in optimized bicarbonate-buffered mineral medium (DSMZ – Medium 721) under anaerobic conditions at 22 °C.

No growing was observed in the absence of ferrous chloride and when sodium acetate was used instead of sodium lactate as carbon source. It is important for interaction experiments with metals to take the cells after defined stages of the growth curve. Therefore, the growth curve of the cells was determined by measuring the optical density at 400 nm and by measuring the total amount of nitrogen (which is a measure for the increased number of cells depending on the time). Both approaches gave similar results. Figure 2.1 shows a typical growth curve measured for *D. äspöensis* in optimized liquid medium. Motamedi and Pedersen report a temperature range for growth from 4 to 35 °C with an optimum within 25 and 30 °C [4]. We choose a temperature of 22 °C for growth. It can be seen in Figure 2.1 that *D. äspöensis* is a relatively slow growing bacterium. We used the increased turbidity (optical density) of the medium as measure for the increased number of cells depending on the time. In the exponential phase, the cells are usually in their healthiest state, and thus they tolerate better changes in their environment. Therefore, to study the interaction of *D. äspöensis* with the selected actinides the cells were grown to the mid-exponential phase (4 days). The biomass was collected by centrifugation and washed three times with 0.9% NaCl. The collected biomass was 1.0 ± 0.2 $g_{dry\ weight}/L$.

2.2 Growth on solid medium

For a better storage of *D. äspöensis* cultures, the attempt was made to cultivate the cells under anaerobic conditions on solid medium.

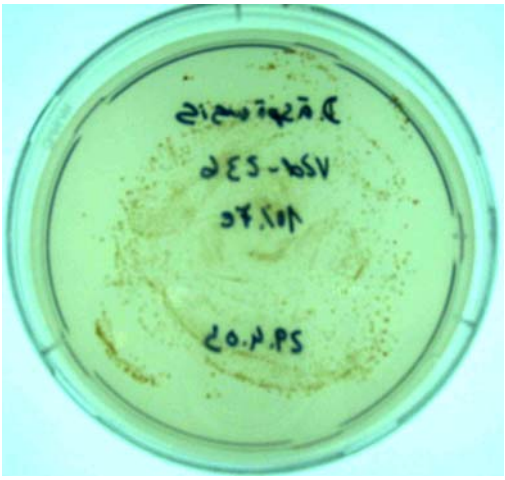

Fig. 2.2: Culture of *D. äspöensis* on solid medium 15 days after inoculation.

15 g/l Bacto-Agar (DIFCO) was mixed with 250 ml of optimized bicarbonate-buffered mineral medium (DSMZ – Medium 721) containing resazurin as a redox indicator. This Agar mixture was sterilized and after cooling down to 50 °C, plates were prepared. The plates were inoculated with a cell suspension of *D. äspöensis* taken at the end of the mid-exponential phase of the growth curve (after 5 days). Those plates were incubated under anaerobic conditions at room temperature. Using this procedure, we could successfully cultivate this less investigated strain on modified solid Agar-medium. Figure 2.2 exhibit the presence of *D. äspöensis* cultures on this solid medium after 15 days. The dark color shows the production of sulfide by the cells.

2.3 Characterization of *D. äspöensis* cultures

2.3.1 Light Microscopy and Scanning Electron Microscopy (SEM)

Microscopy is a major tool for a fast characterization of bacteria based on their individual morphology. Light microscopy was used as routine method to check the purity of the *D. äspöensis* cultures.

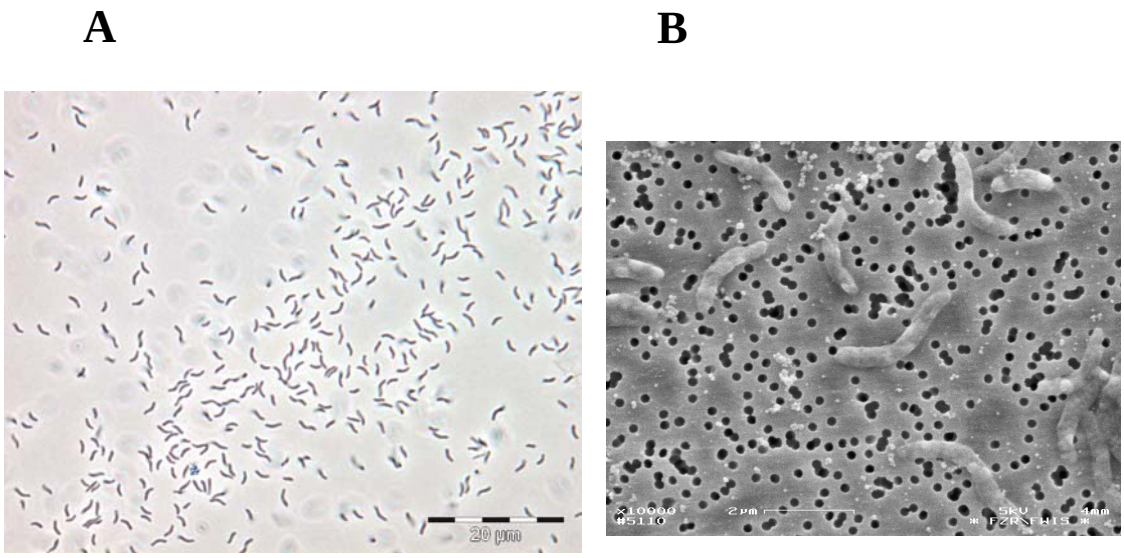

Fig. 2.3.1: Visualization of *D. äspöensis* bacteria (A) using light microscopy and (B) using SEM.

Figure 2.3.1 (A) shows a typical light microscopy image of a liquid culture of *D. äspöensis* cells, whereas Figure 2.3.1 (B) depicts single cells of *D. äspöensis* in more detail. The typical shape of these bacteria, vibrioid and motile cells, can be easily detected. The cells were approximately 0.5 µm in diameter and 1.7 – 2.5 µm long, which is in close agreement with literature values [4]. The cells occurred singly and in chains which is known for lactate as

substrate [4]. Thus the Figure 2.3.1 shows pure cultures of *D. äspöensis*. The light microscopy analyses showed that cells of *D. äspöensis* are able to tolerate oxygen for a certain time. For example, 15 minutes after the sample preparation (6 µl of a liquid culture) on a microscope slide, the majority of the cells were still agile.

2.3.2 Molecular analysis of *D. äspöensis* cultures

Great effort was made to apply molecular biological techniques for a molecular analysis of *D. äspöensis* cells. The first step was the recovery of the total DNA of the bacterial cultures. After that the molecular analysis of the *D. äspöensis* cultures was performed using Amplified Ribosomal DNA Restriction Enzyme Analysis (ARDREA) [5].

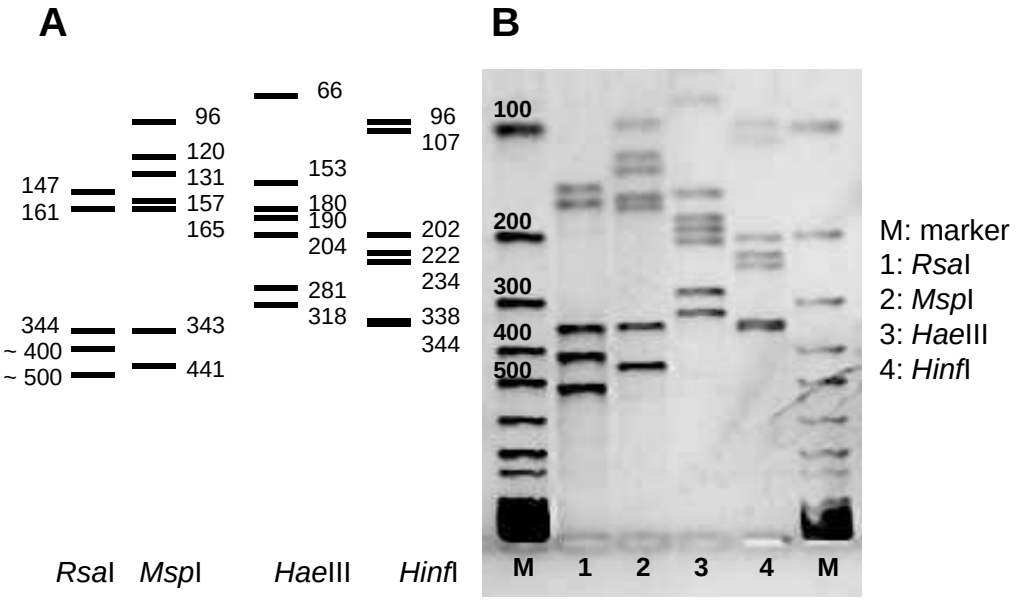

Fig. 2.3.2: Identification of *D. äspöensis* DSM 10631^T based on 16S-ARDREA. A) Schema of the endonuclease-specific ARDREA profiles of *D. äspöensis* drawn on the basis of the sequence analysis of the 16S rRNA-gene. B) Experimentally derived 16S ARDREA patterns of *D. äspöensis* DSMZ 10631^T.

16S rDNA fragments were generated in the total DNA recovered from the bacterial cultures. For this two universal primers 7F and 1541R were used. The resulting PCR amplicons were then digested with the endonucleases *Rsa*I, *Msp*I, *Hae*III and *Hinf*I (see Figure 2.3.2). On the basis of the 16S rDNA sequence of *D. äspöensis*, for every endonuclease a specific pattern was predicted. Figure 2.3.2 summarizes the predicted pattern for every endonuclease marked with A and the experimentally determined pattern marked with B. Both are in agreement and show the purity of the used bacterial cultures.

3 Studies on the interaction of *Desulfovibrio äspöensis* cells with the selected actinides

3.1 Interaction with uranium(VI)

Over the last decade, the interest in interaction processes involving actinides and bacteria has increased markedly. Bacteria are playing an important role in the transport of radionuclides and other heavy metals in nature [6-11]. Within the last years behind the general interest in microbial interactions the interest in sulfate-reducing bacteria (SRB) increased also. These microorganisms are not only able to adsorb toxic metals, they posses also the potential to reduce actinides (actinides soluble in high oxidation states were transferred to lower and less soluble oxidation states), and they can contribute due to their metabolism to the microbial corrosion of e.g., the copper canisters where the radioactive waste is stored. The work on microbial interactions of uranium with SRB was mainly focused on the strains *Desulfovibrio desulfuricans* and *Desulfovibrio vulgaris*. These microbes are able to reduce U(VI) by an enzymatic reaction forming an extracellular precipitate of highly insoluble UO_2 [12, 13]. For *D. vulgaris* the enzyme system responsible for the U(VI) reduction was identified to be cytochrome c_3 [14]. We want to point out that *D. äspöensis* is not closely related to these strains [4], what may result in differences in the interaction mechanism with uranium.

3.1.1 Experimental

The strain *D. äspöensis* was grown under anaerobic conditions in an optimized bicarbonate-buffered mineral medium (DSMZ – Medium 721) as described in chapter 2.1. The biomass was collected by centrifugation and washed three times with 0.9 % NaCl. To study the interaction of *D. äspöensis* with U(VI) the cells were grown to the mid-exponential phase. The collected biomass was 1.0 ± 0.2 $g_{dry\ weight}$/L. The biomass was contacted with U(VI) solution. The experiments were performed in 0.154 M NaCl solutions under nitrogen atmosphere. The U(VI) concentration was varied between 4 mg/l and 162 mg/l. The majority of the experiments were made with 0.01 M lactate in the test solutions. The pH was changed between pH 3 and 8. After defined time intervals samples were taken and analyzed for their uranium content in order to determine the amount of accumulated uranium by the biomass. The speciation of uranium associated with the biomass was investigated using XAS and LIPAS. Flow cytometry experiments in combination with fluorescence microscopy were performed to investigate the toxicity of uranium towards cells of *D. äspöensis*. The cellular

localization of the uranium accumulated by the cells of this bacterium was analyzed by means of TEM/EDX.

3.1.2 Uranium(VI) removal by the biomass

For the first time, we could show the removal of uranium from the solution due to the activity of *D. äspöensis* (Figure 3.1.1 etc.) [15]. In all samples where no cells were added, the uranium concentrations measured by ICP-MS did not differ significantly from the initial values. Ferrous chloride concentrations ranging from 1.9×10^{-6} to 7.5×10^{-7} mol/L in the growing medium do not affect the efficiency of the uranium removal. The main U(VI) removal occurred after the first 24 h. After 72 h, limiting values are reached. Form the measured time dependence of the uranium amount in solution one could speculate that cells of *D. äspöensis* should be able to reduce U(VI). If a pure biosorption takes place limiting values should be reached after a few minutes. The time dependence shown in Figure 3.1.1 could only be fitted to a bi-exponential law. This leads to the conclusion that probably at least two different processes occur after adding the biomass. Additional experiments showed that uranium reduction takes place also without addition of an electron donor.

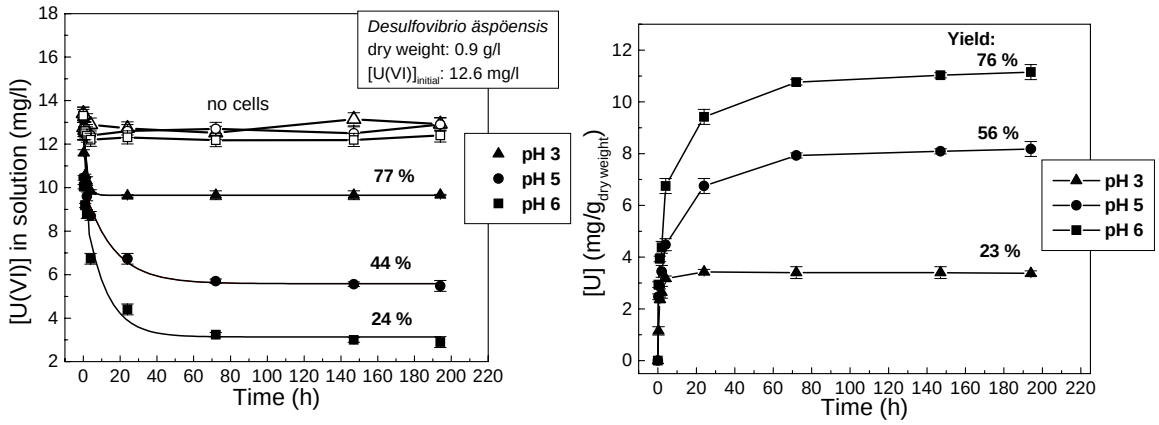

Fig. 3.1.1: Changing U(VI) concentrations ($[U(VI)]_{initial}$ = 12.6 mg/l) in solutions with and without *D. äspöensis* in dependence of the contact time and the pH.

Calculations of the U(VI) speciation in the starting solutions containing 0.01 M lactate showed that at pH 3 the uncomplexed uranyl ion and the first uranyl lactate complex, UO_2HLAC^+, are dominating the U(VI) speciation. Moving to pH 5 the main species are UO_2HLAC^+ and $UO_2(HLAC)_2$. Whereas at pH 6, the binary uranyl hydroxide complexes, e.g., $(UO_2)_3(OH)_5^+$, are the major U(VI) species. The amounts of the different complexes are

changing with the pH and the U concentration. We found no clear dependence of the observed interaction effects from the U(VI) speciation in the starting solutions.
One important result of this project was that the pH limits the uranium removal efficiency.

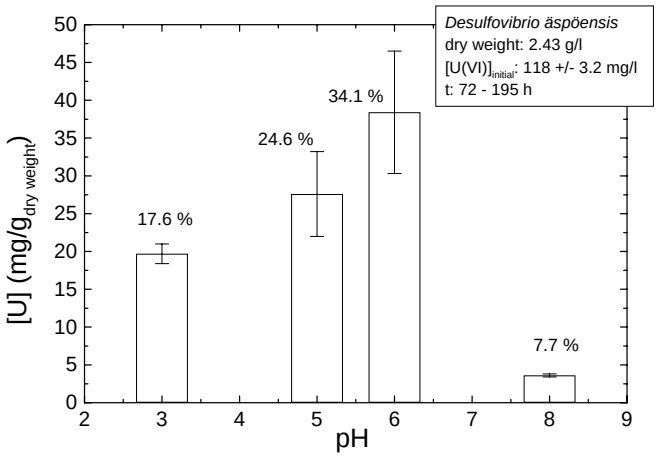

Fig. 3.1.2: Total amount of uranium removed from the solution by *D. äspöensis* as a function of pH.

Low concentrations of uranium were accumulated by the biomass at pH 3 (see Figure 3.1.2). The amount of U bound to the biomass increased with increasing pH according to an increasing deprotonation of the complexing groups (e.g., carboxyl- and phosphate groups) of the bacterial cell envelope. One estimate could be made that the maximum of uranium associated with the biomass would be observed between pH 6 and 7. This is reasonable because this bacterium grows at an optimum pH around 7. At pH 8 a strong decrease in the removal activity, 7%, of the cells was detected.

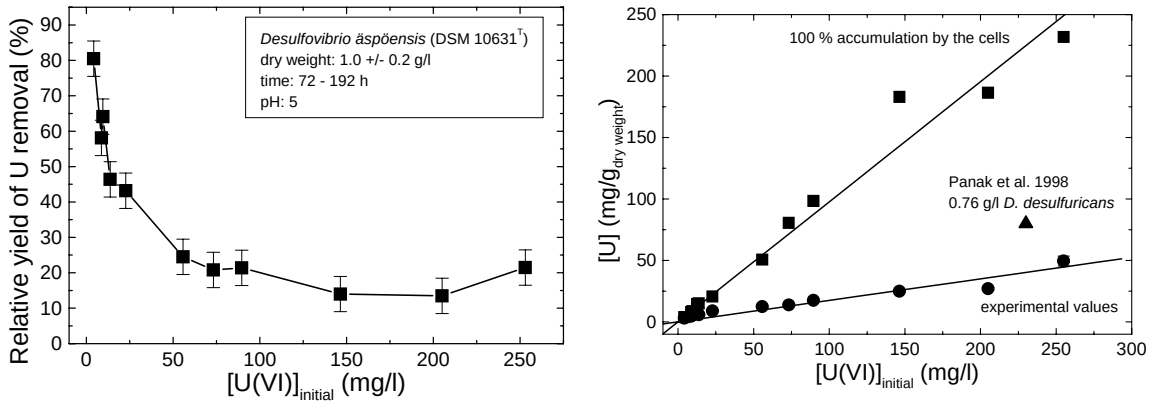

Fig. 3.1.3: Removed uranium from the solution by *D. äspöensis* as a function of the $[U(VI)]_{initial}$ at pH 5.

This study showed that besides the pH the uranium concentration initially present in the solution influences strongly the uranium removal efficiency. At $[U(VI)]_{initial} < 5$ mg/L a removal efficiency of 80% could be achieved. At $[U(VI)]_{initial} > 50$ mg/L, the removal efficiency decreased to a level of 15 to 22%. Comparing our findings with the literature [16, 17], one might speculate that *D. äspöensis* are tolerating less uranium compared to *D. desulfuricans*, to achieve a maximum on removed uranium. The decreased amount of accumulated uranium with increasing initial U concentrations points to the effect of toxicity and metal stress to the cells caused by uranium. On the other hand, we observed with increasing $[U(VI)]_{initial}$ increasing total amounts of removed U by the biomass. On the basis of these results and those found in the literature with *D. desulfuricans* one may speculate that *D. äspöensis* enzymatically reduces U(VI) [12-14, 16, 17]. A detailed investigation of the toxicity of uranium to *D. äspöensis* is summarized in the following chapter.

3.1.3 Toxicity of U(VI) towards *D. äspöensis* studied by flow cytometry and fluorescence microscopy

Flow cytometry (FCM) is a powerful technique with great potential for performing both qualitative and quantitative analyses based on simultaneous measurements of structural and functional parameters of individual cells. In this study, we used the LIVE/DEAD BacLight Kit [18] (stain mixture distinguishes viable bacterial cells from dead ones on the basis of membrane integrity) to investigate the toxicity of uranium towards *D. äspöensis*. The kit contains two nucleic acid stains. The green fluorochrome (Syto 9) is a small molecule that penetrates intact plasma membranes, while the larger red fluorochrome (propidium iodide, PI) penetrates only damaged membranes. Both show fluorescence when bound to DNA, but PI has the higher affinity and replaces Syto 9, thus allowing a clear distinction between cells with intact membrane (green) and dead cells with destroyed membrane (red).

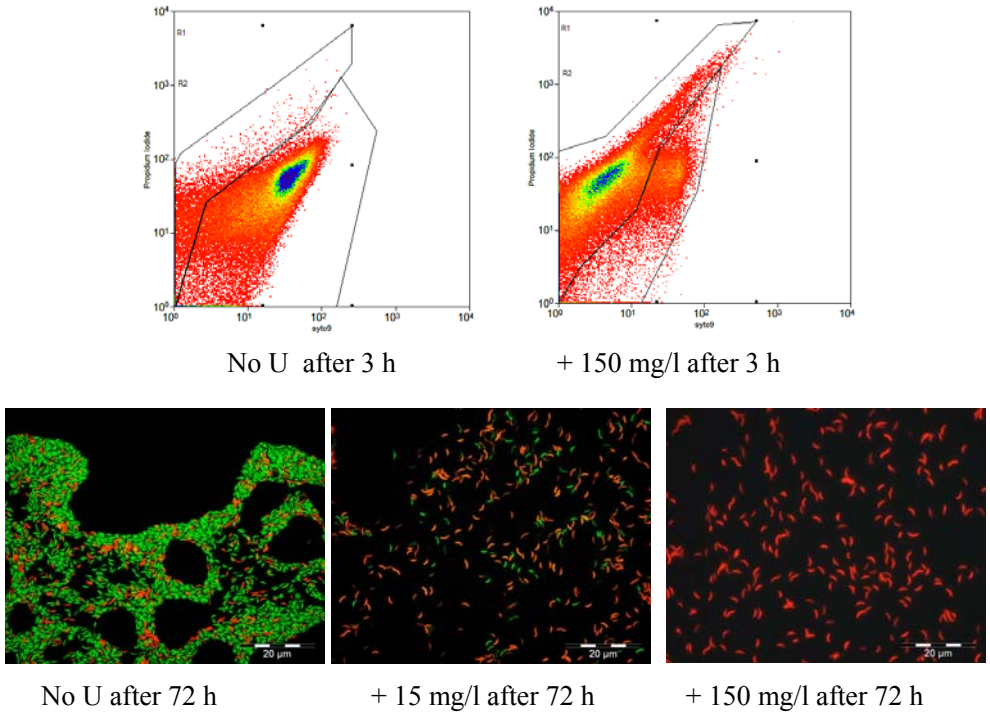

Fig. 3.1.4: FCM (top) and fluorescence microscopy (bottom) analysis of *D. äspöensis* in the absence and the presence of uranium.

To study the toxic effect of uranium on this bacterium, the cells were treated with 2 different concentrations of this metal (15 and 150 mg/L) during 3, 14, 20, 48 and 72 h. After the contact with uranium, cells (1ml) were mixed with 3 µl of a mixture of Syto 9 and propidium iodide (1:1), nucleic acid stains from LIVE/DEAD kit and were incubated in the dark for 15 min at room temperature. Bacterial suspensions incubated in the presence of both stains

simultaneously were analyzed by flow cytometry and fluorescence microscopy for green (i.e., viable) and red (i.e., dead) fluorescence.

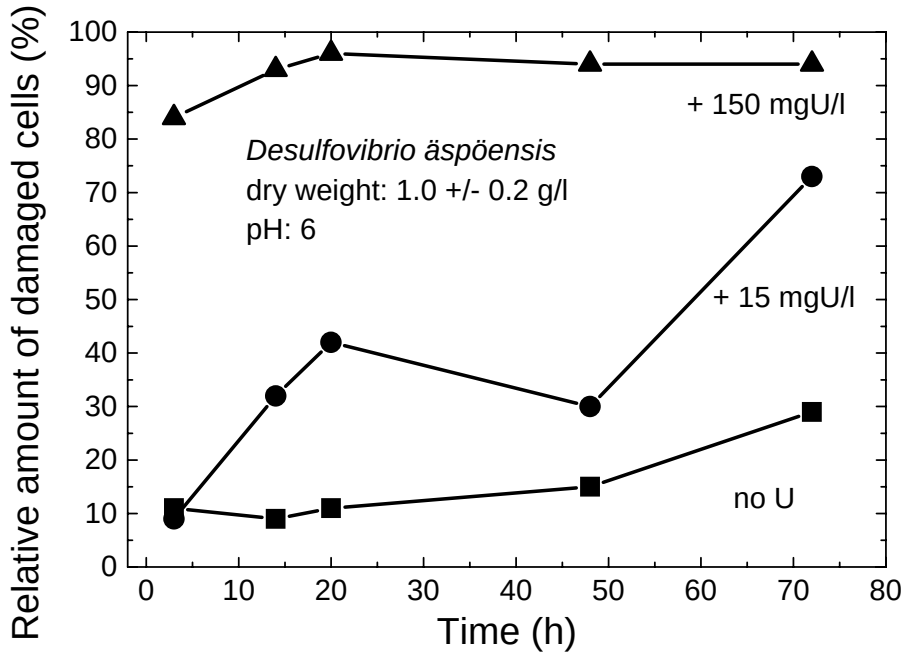

Fig. 3.1.5: Results of the FCM analysis of the viability of *D. äspöensis* in the absence and in the presence of uranium.

In the absence of uranium, and after 48 and 72 h of incubation, 80 and 75% of the cells exclude propidium iodide (Figures 3.1.4 and 3.1.5). This fluorescent dye is concentrated by microbial cells in an energy-dependent fashion. Hence, staining with Syto 9 and subsequent flow cytometric analysis is one approach to measure metabolic active cells. This observation is illustrated by the fluorescence microscopy image where most of the cells having intact cell membranes and staining fluorescent green (Figure 3.1.4). However, after 72 h of cell incubation with 15 and 150 mg/l of uranium, 30 and only 5% of the cells exclude propidium iodide (live cells), respectively (see Figures 3.1.4 and 3.1.5). Already after 3 h of incubation with 150 mg/l of uranium, only 16% of the cells having intact cell membranes. Flow cytometry showed that as a result of the uranium stress the cell membrane is damaged. But at least at the lowest uranium concentration investigated, the cells should be able to reduce uranium by an enzymatic reaction within the first 72 h of contact time.

3.1.4 Speciation of U associated with the biomass investigated by means of XAFS Spectroscopy and LIPAS

X-ray Absorption Fine Structure (XAFS) spectroscopy

After culturing of *D. äspöensis* in optimized growth medium, the bacterial cells were obtained by centrifugation. They were washed and re-suspended in a solution of 0.9% NaCl. Two samples were prepared in a first set of measurements. The amount of accumulated uranium was 42.4 $mg/g_{dry\ weight}$ and 10.7 $mg/g_{dry\ weight}$ at pH 5 and 6, respectively. After shaking the samples for 7 days under nitrogen atmosphere, the biomass was separated by centrifugation, washed with 0.9% NaCl solution, and sealed in polyethylene cuvettes. The interaction time in the second set of experiments was shortened to 48 and 168 h. Here, the amount of accumulated uranium ranged between 1.37 and 37.35 $mg/g_{dry\ weight}$.

The XAS data were recorded at the Rossendorf Beamline (ROBL) [19] at the ESRF in Grenoble, France. The U L_{III}-edge X-ray absorption spectra were collected in fluorescence or transmission mode at room temperature. A Si(111) double-crystal monochromator was used in fixed-exit mode. Several EXAFS scans were collected from each sample and averaged.

Data analysis was performed according to standard procedures [20] using EXAFSPAK software [21]. The program FEFF6 [22] was used to calculate theoretical scattering amplitudes and phase-shift functions.

XANES spectroscopy is one method to distinguish between different oxidation states of an absorbing atom. U(VI) samples can be easily detected by a characteristic shoulder approximately 20 eV above the white line. This feature (marked with an arrow in Figure 3.1.6) results from multiple scattering processes within the linear uranyl unit (O=U=O). It is only present in the case of uranium(VI). The reduced amplitude of this shoulder of the bacterial sample clearly indicates the presence of uranium(IV) formed by the activity of the cells. To conclude in one sample, we were successful in detecting uranium in both oxidation states +4 and +6 as depicted in Figure 3.1.6. To determine the amounts of U(IV) and U(VI) present in the bacterial sample, we applied the Factor Analysis described in [23]. The calculations revealed a mixture containing 20% U(IV) and 80% U(VI). To the knowledge of the authors, this is the first experimental proof that *D. äspöensis* can reduce U(VI) to U(IV).

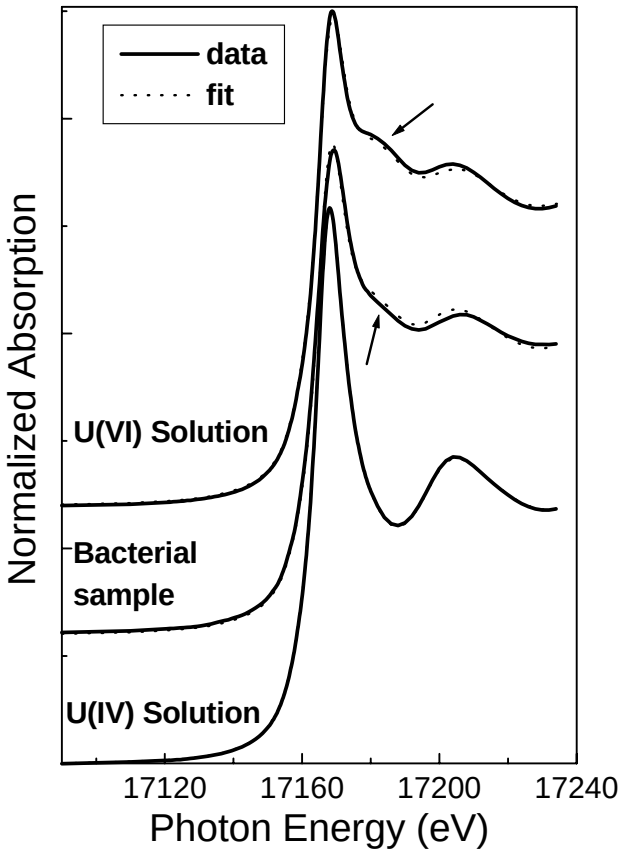

Fig. 3.1.6: U L_{III}-edge XANES spectra of 0.03 M U(IV) and 0.04 M U(VI) reference solutions in 1 M $HClO_4$ and after bacterial reduction of U(VI) ([U] 42.4 $mg/g_{dry\ weight}$, interaction time 7 days at pH 5). Solid line: experiment; dots: calculated spectrum.

On the other hand, this study shows the difficulties to detect U(IV) formed by microorganisms in the presence of large amounts of U(VI). Unfortunately, the XANES spectra of all other samples showed that the main part of the uranium occurred as U(VI). The amount of U(IV) was always below 5%. Our investigations indicated that *D. äspöensis* interacts with U in a complex mechanism consisting of biosorption, bioreduction and bioaccumulation. It seems that in these samples the biosorption of U(VI) on the cell envelope is the dominating process. The following enzymatic reduction of U(VI) to U(IV) is somehow inhibited. One reason for the difficulties in detecting U(IV) in these samples could be a re-oxidation of U(IV) to U(VI).

In the following we are describing the structure of uranyl biosorbed on the cell envelope of the Gram-negative bacterium *D. äspöensis*. Figure 3.1.7 shows a typical uranium L_{III}-edge

EXAFS spectrum and the corresponding Fourier transform of the uranium species formed by *D. äspöensis* at pH 5.

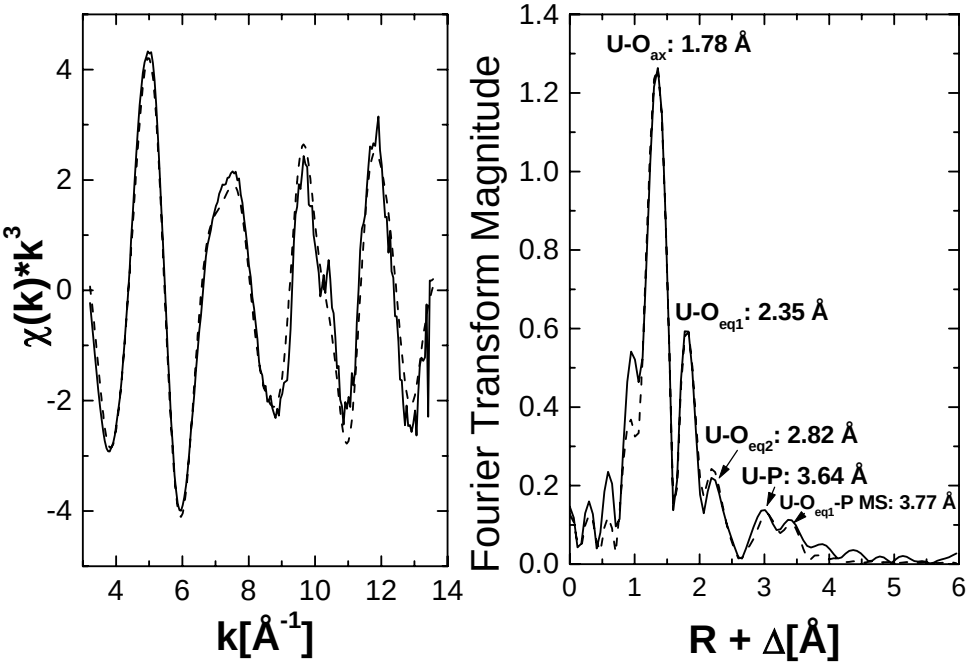

Fig. 3.1.7: U L_{III}-edge k^3-weighted EXAFS spectrum and corresponding FT of the *D. äspöensis* uranium complexes ([U] 10.81 mg/$g_{dry\ weight}$, interaction time: 48 h, pH 5).
Solid line: experiment, dashed line: fit.

The EXAFS data evaluation yielded a relatively short U-O_{eq1} distance of 2.35 Å. This indicates an intensive interaction of U(VI) with the surface of the bacteria. The U-P distance of 3.64 Å points to a coordination of U(VI) in a mainly monodentate mode to phosphate groups of the cell envelope. Organic phosphato-groups can originate, e.g., from the lipopolysaccharide (LPS) layer and from phosphoryl residues of the polar head of phospholipids in the outer membrane of the cell envelope [16]. We have noticed the close agreement of the structural parameters determined for U in this study with those recently reported for other Gram-negative bacteria, e.g., *Acidithiobacillus ferrooxidans* [17, 18].

Laser-induced photoacoustic spectroscopy (LIPAS)

In this study we are applying a new method, LIPAS, for the identification of U(IV) associated with the biomass. To our knowledge there are no studies so far exploring the speciation of actinide-bacteria complexes/compounds using this spectroscopic technique. LIPAS is a

powerful tool to study the spectroscopic properties of actinides at very low concentrations [27]. A further advantage of this method is the detection of U(IV) in the presence of U(VI).
The biomass was collected by centrifugation and washed three times with 0.9 % NaCl. To study the interaction of *D. äspöensis* with U(VI) the cells were grown to the mid-exponential phase. The collected biomass was 0.8 $g_{dry\ weight}$/l. Two parallel samples were prepared. In sample A, the cells were incubated with 15 mg/l U(VI) in solution at pH 5. In sample B the uranium concentration used was 150 mg/l. After shaking the samples for 72 h under nitrogen atmosphere, the LIPAS spectra were measured. The design of LIPAS is described in [27].
We are presenting the first interpretation of the LIPAS data measured in a biological system. The LIPAS spectra of samples A and B are summarized in the Figure 3.1.8.

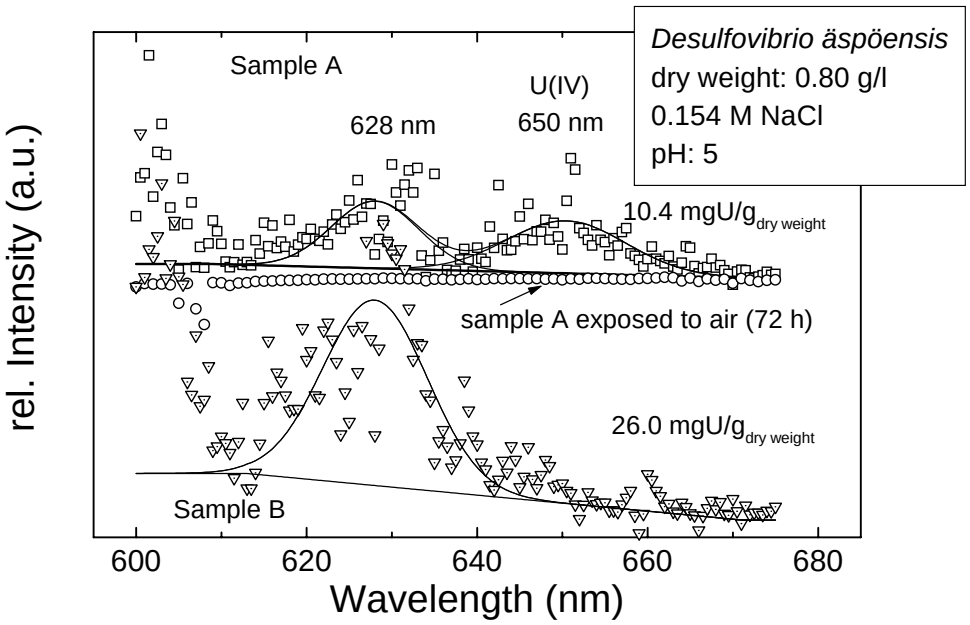

Fig. 3.1.8: LIPAS spectra of uranium in suspensions of *D. äspöensis*.

The spectra of the bacterial samples are different. In principle, the only difference between both samples is the uranium concentration present in the medium. The reasons for the observed varieties are not fully understood. In the spectrum of sample A, we could identify two absorption bands centered at 628 and 650 nm. A comparison with the literature showed that U(IV) shows characteristic absorption maxima at 625.5, 649.1 and 671.7 nm [27]. Especially from the detected absorption band at 650 nm, we are concluding the presence of U(IV) due to the activity of the cells of *D. äspöensis*. At the moment, we can not quantify the amount of U(IV). When the sample A was exposed to air for 72 h, the absorption bands at 628 and 650 nm disappeared due to re-oxidation of U(IV) and because the bacteria are damaged

by the oxygen. This gives further evidence that the existence of U(IV) in the original sample A was connected to the activity of the bacterial cells. After the XAS results described above, this is the second experimental proof that *D. äspöensis* bacteria are able to reduce U(VI) to U(IV) by an enzymatic reaction.

In sample B, where the amount of uranium was 10 times higher and possibly toxic to the bacterial cells, we could not clearly identify the formation of U(IV). The absorption band at 650 nm, which is a strong indication for U(IV), is missing. As a result from additional measurements, we cannot clearly assign the absorption band at 628 nm to the presence of U(IV). The experiments are indicating that the reduction of U(VI) by this novel SRB strain is possibly related with the occurrence of vital cells. Using flow cytometry in combination with fluorescence microscopy, we could demonstrate the toxicity of uranium at these concentrations to the cells of *D. äspöensis* (see chapter 3.1.3). In a system containing 150 mg/l of U, more than 80% of the cells showed damaged membranes already after a contact time of 3 h. If the uranium concentration in the medium is reduced to 15 mg/l approximately 30% of the cells are still vital after 72 h of interaction. The toxicity of uranium at concentrations larger than 15 mg/l might be one reason why the detection of U(IV) failed in sample B. This study shows again the complexity of the interaction mechanism of uranium with *D. äspöensis*.

3.1.5 Localization of the uranium associated with the biomass using TEM/EDX

Transmission electron microscopy (TEM) is a useful technique to localize and identify radionuclides deposited within or around microbial cells. Energy dispersive X-ray analysis (EDX) can provide elemental information via the analysis of X-ray emissions stimulated by a high energy electron beam [28].

After the uranium accumulation was finished (0.63 mM, pH 5 for 48 h), the bacterial cells were fixed in 2.5% glutaraldehyde in 0.1 M cacodylate buffer (pH 7.2) for 2 h at 4 °C and then washed three times with the same cacodylate buffer. The cell pellets were fixed for 60 min at 4 °C in 1% OsO_4 in cacodylate buffer before being dehydrated with ethanol and embedded in Spurr resin.

Thin sections (0.25 µm) cut with a diamond knife on a Reichert Ultracut S ultramicrotome were supported on copper grids and coated with carbon. Samples were examined with a high resolution Philips CM 200 transmission electron microscope (at an acceleration voltage of 200 kV), equipped with microanalysis system, by EDX.

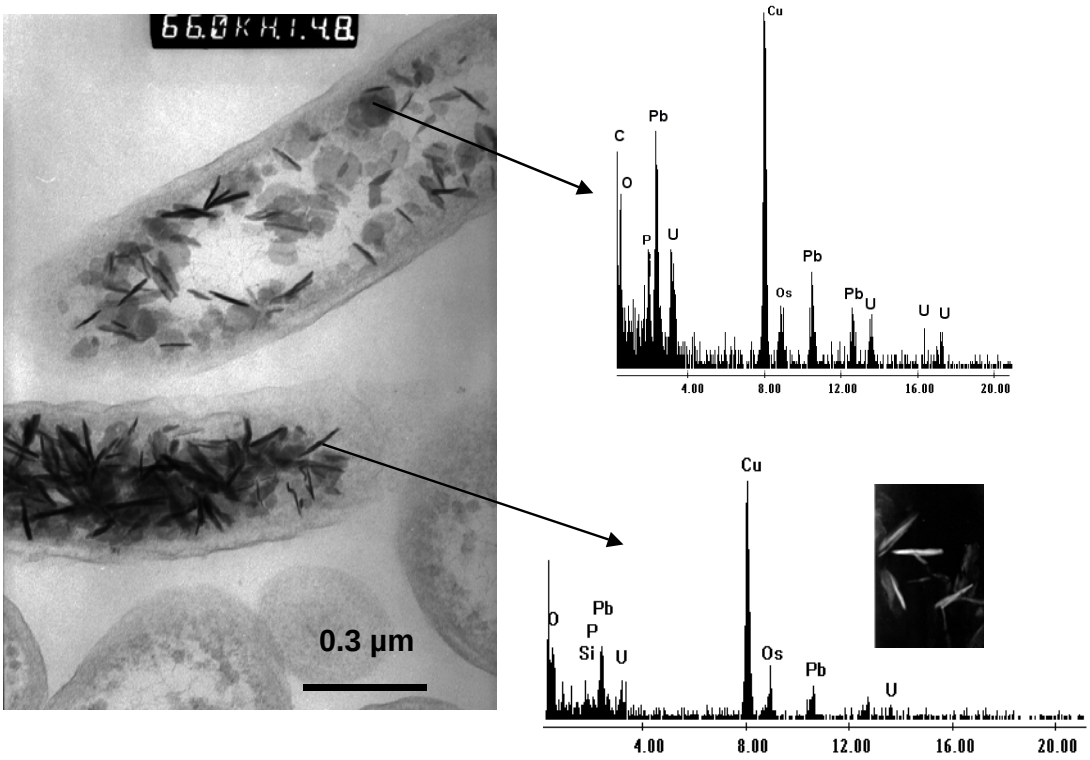

Fig. 3.1.9: TEM and EDX analysis of the cellular localization of uranium accumulated by the cells of *D. äspöensis*.

TEM and EDX analysis of cells of *D. äspönensis* exposed to 150 mg/l U(VI) in 0.01 M lactate solution allow the detection of electron-dense accumulates essentially within the cytoplasm and associated with or close to the membrane system. Interestingly, some cells are completely occupied by these accumulates without presenting visually damaged membranes as seen in the Figure 3.1.9. The EDX spectrum derived from the U deposits indicated that they are composed of oxygen (O), phosphorus (P) and uranium (U). The high copper (Cu) peak is from the EM grid used to support the specimen. The lead (Pb) peak originated from the lead citrate solution which was used in order to improve the visualization of the uranium-treated cell thin sections. To summarize, the cells of *D. äspöensis* accumulate uranium intracellulary, presumably, as phosphate compounds after 48 h contact with this metal. Flow cytometry (see chapter 3.1.3) showed that as a result of the uranium stress the cell membrane is damaged and uranium can penetrate inside the bacterial cells.

3.1.6 Summary of the uranium results

In this study, we could show for the first time the removal of U(VI) due to the activity of the cells of *D. äspöensis*. Three parameters are influencing the removal efficiency of U(VI): a) the interaction time, b) the pH, and c) the initial uranium concentration, $[U]_{initial}$, present in the test solutions.

The main U(VI) removal occurred after the first 24 h and limiting values were reached after 72 h. The time dependence of the U concentration in solution could only be fitted to a bi-exponential law. This leads to the conclusion that at least two different processes occur after adding the biomass. The amount of U bound to the biomass increased with increasing pH from 3 to 6. This is reasonable because this bacterium grows at an optimum pH around 7.3. Approximately 25 $mg/g_{dry\ weight}$ of U were bound after 72 h at pH 6 and $[U]_{initial}$: 162 mg/l. However, a strong decrease of the amount of accumulated uranium was observed at pH 8.

At low $[U]_{initial}$ of < 5 mg/l, approximately 80% of the provided uranium was accumulated by the biomass. This value decreased to about 20-25% at $[U]_{initial}$ of > 120 mg/l. Comparing our findings with the literature [16, 17], one might conclude that *D. äspöensis* are tolerating less uranium compared to *D. desulfuricans*, to achieve a maximum on removed uranium. On the other hand, we observed with increasing $[U]_{initial}$ increasing total amounts of removed U by the biomass. Flow cytometry analysis demonstrated clearly the toxicity of U(VI) towards *D. äspöensis*. At 150 mg/l of U, more than 80% of the cells showed damaged cell membranes already after 3h of interaction time. As a consequence, we could demonstrate that the cells accumulate uranium intracellulary by TEM/EDX. Using XANES and LIPAS, we observed indications for the formation of U(IV) due to the activity of the biomass.

The results are indicating a complex interaction mechanism consisting of biosorption, bioreduction, and bioaccumulation.

3.2 Interaction with curium(III)

The aim of this part of the project is to explore interaction processes of the SRB *D. äspöensis* with trivalent actinides. As representative for trivalent actinides curium was chosen. Due to its fluorescence spectroscopic sensitivity, speciation studies are possible at the trace concentration level. The limit of detection for Cm^{3+} (aq) by time-resolved laser fluorescence spectroscopy (TRLFS) is $5x10^{-12}$ mol/l [29]. A summary of the spectroscopic properties of Cm(III) is given in [29]. TRLFS has been proven as a powerful tool to study solution chemistry of curium in the presence of inorganic and organic ligands [29-38] as well as surface complexation reactions of Cm(III) onto different minerals [39-42].

To our knowledge, there are no spectrophotometric data available for interactions of Cm(III) with bacteria and especially with sulfate-reducers of the type *Desulfovibrio*. Recently Ozaki et al. [43] reported results concerning the association of Eu(III) and Cm(III) with the Gram-positive bacterium *Bacillus subtilis* and with the archaeon *Halobacterium salinarum*. The authors investigated the coordination state of Eu(III) sorbed onto these two different kinds of microorganisms at pH-values between 3 and 6 by using TRLFS. Eu(III) forms inner-sphere and outer-sphere complexes with the cells of these organisms. During the sorption process the number of water molecules in the first coordination sphere of Eu(III) decreases from nine, found for the Eu^{3+} aquo ion, to four found for the Eu(III) sorbed on *B. subtilis*. Spectrophotometric data for curium interaction with *B. subtilis* and *H. salinarum* are not published. In this chapter, we report new data for the surface complexation of Cm(III) onto the cell envelope of *D. äspöensis* determined by TRLFS at 25 °C and in 0.154 M NaCl medium [44]. The interaction process of the bacteria and Cm(III) was investigated in the pH range from 3.00 to 7.55.

3.2.1 Experimental

The bacteria were grown and characterized as described in chapter 2. A stock solution of the long-lived curium isotope Cm-248 ($t_{1/2}$ = $3.4x10^5$ years) was used. This solution had the following composition 97.3% Cm-248, 2.6% Cm-246, 0.04% Cm-245, 0.02% Cm-247, and 0.009% Cm-244 in 1.0 mol/L $HClO_4$. The experiments were performed in a glove box under N_2 atmosphere at 25 ˚C. As a background electrolyte 0.154 M NaCl was used. To avoid carbonate complexation of Cm(III) carbonate free water and NaOH solution was used. The Cm(III) concentration was fixed to $3x10^{-7}$ M in all TRLFS measurements. The pH was

measured using a glass electrode (type: Mettler Toledo InLab 427) calibrated in H^+ concentration units. The pH was changed between 3.00 and 7.55 by adding analytical grade NaOH or $HClO_4$. 0.25 ml of bacterial suspension and 1.25 ml of Cm(III) working solution were combined and equilibrated for 72 h. The samples were shaken periodically.

The TRLFS spectra were recorded at 25ºC using a flash lamp pumped Ti:sapphire laser (Elight, Titania). Details on the experimental set-up are summarized in [37]. The excitation wavelength was 395 nm using a laser energy of 2 mJ controlled by a photodiode. The fluorescence emission spectra were detected by an optical multi-channel analyzer. The system consists of a monochromator and spectrograph (Oriel; MS 257) with a 300 or 1200 lines mm^{-1} grating and an ICCD camera (Andor). The Cm(III) emission spectra were recorded in the 500-700 nm (300 lines mm^{-1} grating) and 570-650 nm (1200 lines mm^{-1} grating) ranges, respectively. A constant time window of 1 ms was used. For time depended emission decay measurements the delay time between laser pulse and camera grating was scanned with time intervals between 10 and 20 µs.

3.2.2 Results and discussion

Figure 3.2.1 shows fluorescence emission spectra of $3x10^{-7}$ M Cm(III) in aqueous solution in presence of *D. äspöensis* at various pH. The spectra of Cm(III) in solution at pH 3.00 and at pH 7.55 in absence of bacteria are also shown. At pH 3 only the emission band of the Cm^{3+} aquo ion with a peak maximum at 593.8 nm was detected. At pH 7.55 a red shoulder is visible in the spectrum of Cm(III) indicating the formation of the first hydrolysis complex $Cm(OH)^{2+}$. This is in agreement with studies of Fanghänel et al. confirming that the first hydrolysis complex $Cm(OH)^{2+}$ is formed at pH > 6 in carbonate free solutions [30, 45]. From the pH depended emission data of Cm(III) in presence of bacteria (Figure 3.2.1), we conclude that hydrolysis plays no role in the reaction mechanism. When hydrolysis occurs all of the Cm(III) is already sorbed onto the cell envelope of the bacteria. 0.093 mg Cm(III) are bound to the biomass per g dry weight at pH 7.55. In all samples with cells at pH < 3.35, the emission band of the Cm(III) aquo ion dominates the fluorescence emission spectra. Starting at pH 3.35 the intensity of the 593.8 nm peak decreases with increasing pH and a second peak appears with a peak maximum at 600.1 nm. This peak dominates the emission spectra at pH > 4.1. We interpret the pH dependence of the emission spectra as biosorption, forming an inner-sphere surface complex of Cm(III) onto the cell envelope of *D. äspöensis*.

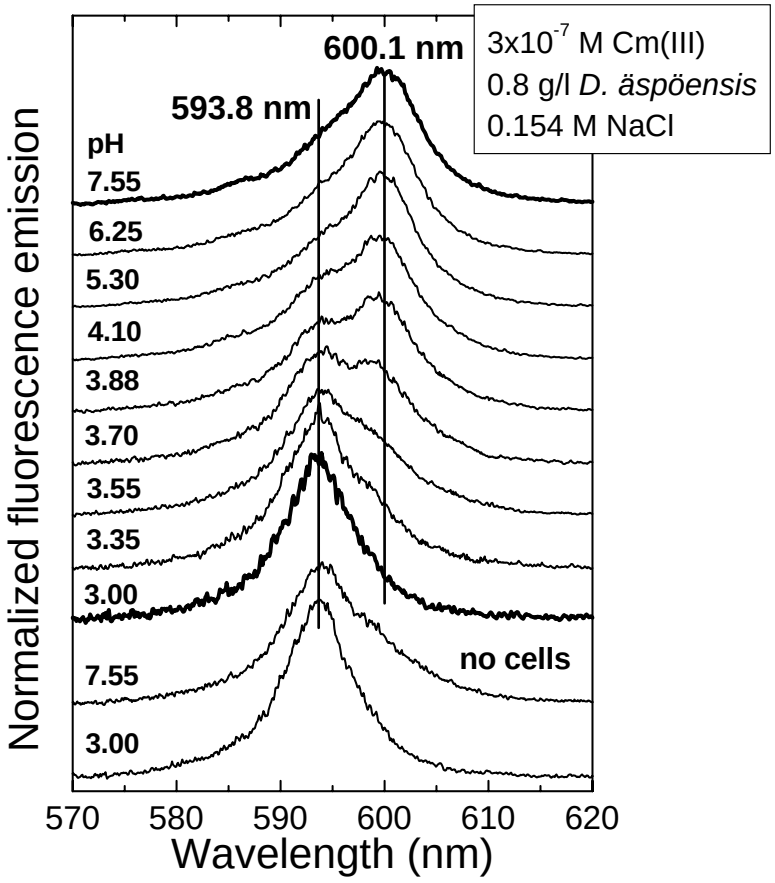

Fig. 3.2.1: Fluorescence emission spectra of $3x10^{-7}$ M Cm(III) in a suspension of *D. äspöensis* in 0.154 M NaCl at different pH values; the spectra are scaled to the same peak area.

We applied the factor analysis described in [23] to calculate the contributions of the pure components to the measured composite spectra. The factor analysis yielded that the composite spectra can be described by only two components. The spectra of these single components derived by deconvolution of the mixed spectra (Figure 3.2.1) are shown in Figure 3.2.2 A. A plot of the experimentally determined speciation based on the deconvoluted spectra (Figure 3.2.2 A) is presented in Figure 3.2.2 B.

The relative fluorescence intensity (FI) of the Cm(III)-*D. äspöensis*-surface complex normalized to that of the Cm(III) aquo ion, is 2.6. This value is comparable with FI values found for complexes with purified humic and fulvic acid isolated from the Gohy 573 groundwater [36, 33].

Desorption experiments were performed to check the reversibility of the biosorption of Cm(III) onto functional groups of the *D. äspöensis* cell envelope. $HClO_4$ was added to a

Cm/bacteria containing sample at pH 6 to get pH 3. After a few minutes, TRLFS measurements confirmed that the emission band of the Cm(III) surface complex moved from 600.1 nm to 593.8 nm. The detection of the Cm(III) aquo ion indicates the reversibility of the sorption reaction. One may conclude from these findings that Cm(III) was sorbed on the surface of these bacteria. No indication was found for an accumulation of Cm(III) inside the bacterial cells. In contrast to the here presented results for Cm(III), there is evidence for uranium accumulation inside the cells of *D. äspöensis* but at higher metal ion concentration (>$6.6x10^{-5}$ M and >10.7 mg $U/g_{dry\ weight}$) (see chapter 3.1). The much lower metal concentration used in this study, $3x10^{-7}$ M corresponding to 0.093 mg $Cm/g_{dry\ weight}$, might be one reason for the absence of an accumulation of Cm(III) inside the cells. Taking only the metal concentration into consideration, the cell membrane should be intact also at contact times larger than 72 h.

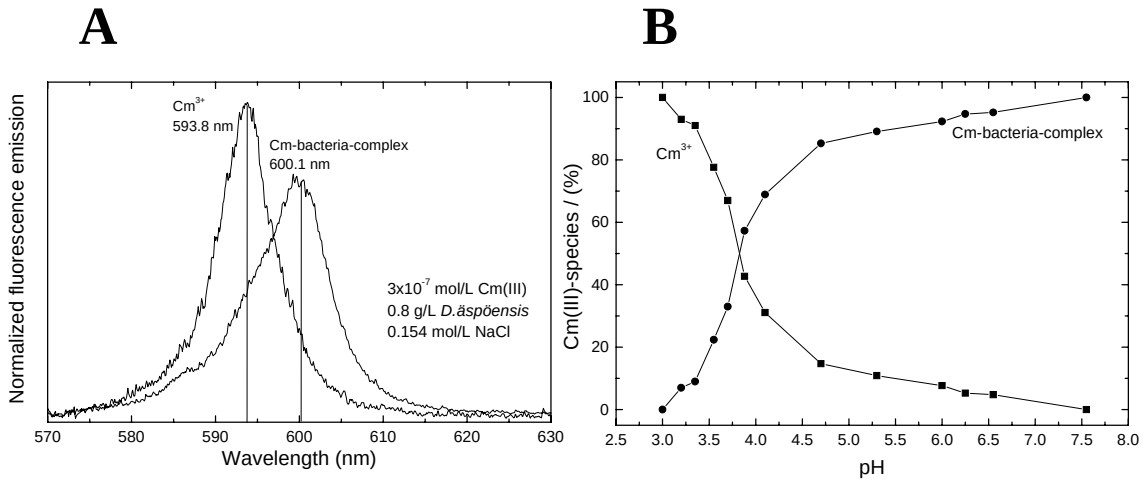

Fig. 3.2.2: A) TRLFS spectra of component 1: Cm^{3+} and component 2: Cm-*D. äspöensis*-surface complex as derived by peak deconvolution; the spectra are scaled to the same peak area. B) Experimental species distribution of the Cm(III)-*D. äspöensis* system as a function of pH, determined by using a factor analysis program.

Centrifugation experiments (12000 rpm, 60 minutes) revealed that more than 95% of Cm(III) is sorbed onto the bacteria at pH 6. Centrifugation of the sample at pH 3 had no influence on the emission spectra meaning that all of the Cm(III) exists as Cm^{3+} aquo ion in the solution.
Lifetime measurements provide information on the composition of the first coordination sphere of Cm(III) and on the kinetics of the complex formation reactions [30]. Fluorescence decay rates are a result of radiative and nonradiative processes. The Cm(III) aquo ion is characterized by a measured lifetime of 68±3 µs [46-48]. Increasing lifetimes of Cm(III)

species are reflecting the exclusion of water molecules out of the first coordination sphere of the Cm(III) due to complex formation reaction. A linear correlation between the decay rate and the number of H_2O molecules in the first coordination sphere of Cm(III) was found by Kimura and Choppin [49]. 68 µs [46-48] measured for the Cm(III) aquo ion corresponds to nine water molecules, and a value of 1300 µs corresponds to zero water molecules in the first coordination sphere of Cm(III) [50]. The fluorescence lifetime (luminescence decay) of Cm(III) in the *D. äspöensis* suspensions at various pH was determined (Figure 3.2.3).

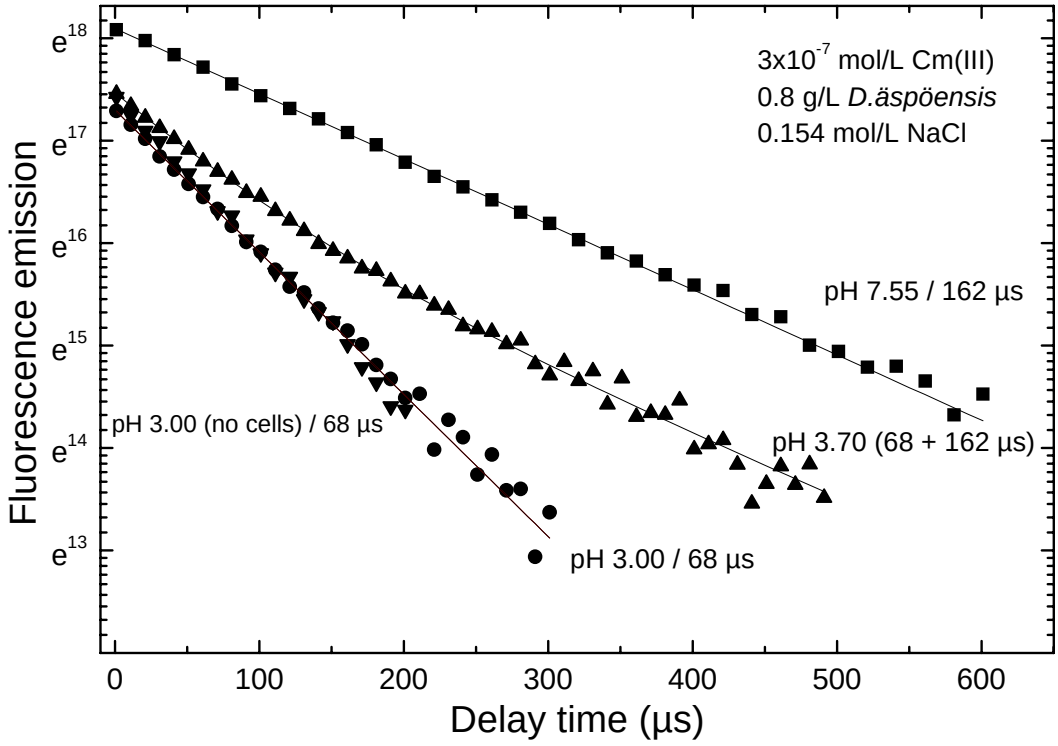

Fig. 3.2.3: Fluorescence emission lifetimes of $3x10^{-7}$ M Cm(III) in *D. äspöensis* suspension at various pH; mono- and bi-exponential decay behavior.

In presence of both species at pH 3.7, the fluorescence emission decay shows a bi-exponential behavior. This indicates that the lifetime of the excited state of Cm(III) is short compared to the exchange rate between the Cm(III) aquo ion and the surface complex [30]. For the Cm^{3+} aquo ion 68 µs were calculated, whereas the Cm-*D. äspöensis*-surface complex is characterized by a long fluorescence emission lifetime of 162±5 µs. According to the Kimura & Choppin equation a lifetime of 68 µs corresponds to nine water molecules in the first Cm(III) coordination sphere and a lifetime of 162 µs corresponds to three water molecules in the actinide first hydration shell. Ozaki et al. observed a decrease of water molecules in the

Eu(III) first hydration shell to four as a result of the interaction with *B. subtilis* at pH 5.9 [43]. In contrary, in the case of the archaeon *H. salinarum* the number of coordinated water molecules increased from 3 to 6 with an increase of pH from 3.5 to 5.8 [43]. It seems that the complexation of Cm(III) by *D. äspöensis* is similar to those of Eu(III) with *B. subtilis* and differs significantly from the case of *H. salinarum*. The latter can be explained with the significant differences in the cell envelope structures between bacteria and archaea. The dehydration of Cm(III) by sorption onto the bacteria can be explained by the interaction process of Cm(III) and the cell envelope of *D. äspöensis*. In general, bacteria can be divided into two major groups, called Gram-positive and Gram-negative depending on differences in their cell envelope structure. *D. äspöensis* belongs to the Gram-negative bacteria. The cell envelope of the Gram-negative bacteria shows a complex multilayered structure containing among other functional groups: hydroxyl, carboxyl and phosphate groups [51]. Organic phosphato-groups can originate, e.g., from the lipopolysaccharide (LPS) layer and from phosphoryl residues of the polar head of phospholipids in the outer membrane. The LPS layer has been implicated as the major source of metal binding in the group of Gram-negative bacteria [24, 52]. The long fluorescence lifetime is a main difference compared to the results published for Cm(III) complexes with humic [32-34] and fulvic acids [36] as well as determined for the first sorption complex of Cm(III) onto clays (smectite and kaolinite) and γ-alumina [40, 41]. This findings and other investigations of Gram-negative bacteria with actinides, e.g., uranium [53, 54, 25] and plutonium [55], may indicate rather an interaction of Cm(III) with organic phosphato-groups of the cell envelope than with carboxylic groups.

3.2.3 Interaction of Cm(III) with relevant model compounds

For a better understanding of the biosorption process of Cm(III) onto the cell envelope of the sulfate-reducing bacterial strain *D. äspöensis* on a molecular level, we investigate the complexation of curium with selected bioligands of relevant functionalities as model compounds. The spectroscopic studies of uranium and other actinide complexes in several biological systems like microorganisms [25, 55, 56] and plants [57] indicated that one functionality, most likely the phosphate group, might be responsible for complexation.

The first model system investigated was Cm(III)-Adenosine 5'-triphosphate (ATP). The ATP molecule can interact with metal ions via the oxygen atoms from the triphosphate chain and the nitrogen atoms of the purine nucleus (N-1, N-3 and N-7). ATP is an important enzymatic compound in the life sciences. This molecule is the major source of energy for cellular reactions. The amount of adenosine phosphates in living systems lies in the 2-10 millimolar concentration range [58]. The fact that a special ATP-synthesizing enzyme can be located in membrane systems of cells [59] points to the importance of ATP for a better understanding of biosorption processes of actinides on cell membranes of microorganisms. Imaginable would be also that heavy metals bound to adenosine phosphates can be transported into living cells and than deposited. Moreover, complexes of ATP with heavy metals can influence the behavior of some enzymes which catalyze important biochemical reactions.

Presently, little is known about the complexation of ATP with actinides. Stability constants for the formation of NpO_2ATP^{3-}, NpO_2HATP^{2-} and UO_2ATP^{2-} are reported in [60, 61]. However, the complex formation with trivalent actinides is unknown up to now. Therefore, we present the results of curium(III) complexation with ATP, obtained by TRLFS [38].

Experimental

Adenosine 5'-triphosphate disodium salt was purchased from ACROS ORGANICS (analytical grade). The experiments were performed under N_2 atmosphere at 25 ˚C. As a background electrolyte 0.154 M NaCl was used. [Cm(III)] was fixed to $3x10^{-7}$ M. [ATP] was varied between $3x10^{-7}$ and $1.5x10^{-4}$ M. The pH was changed between 1.5 and 7.0. The TRLFS spectra were recorded using a flash lamp pumped Ti:sapphire laser (Elight, Titania) as described above.

Results and discussion

Fluorescence emission spectra of $3x10^{-7}$ M Cm(III) with $3x10^{-6}$ M ATP in 0.154 M NaCl in the pH range 1.5 to 7.0 are shown in Figure 3.2.4.

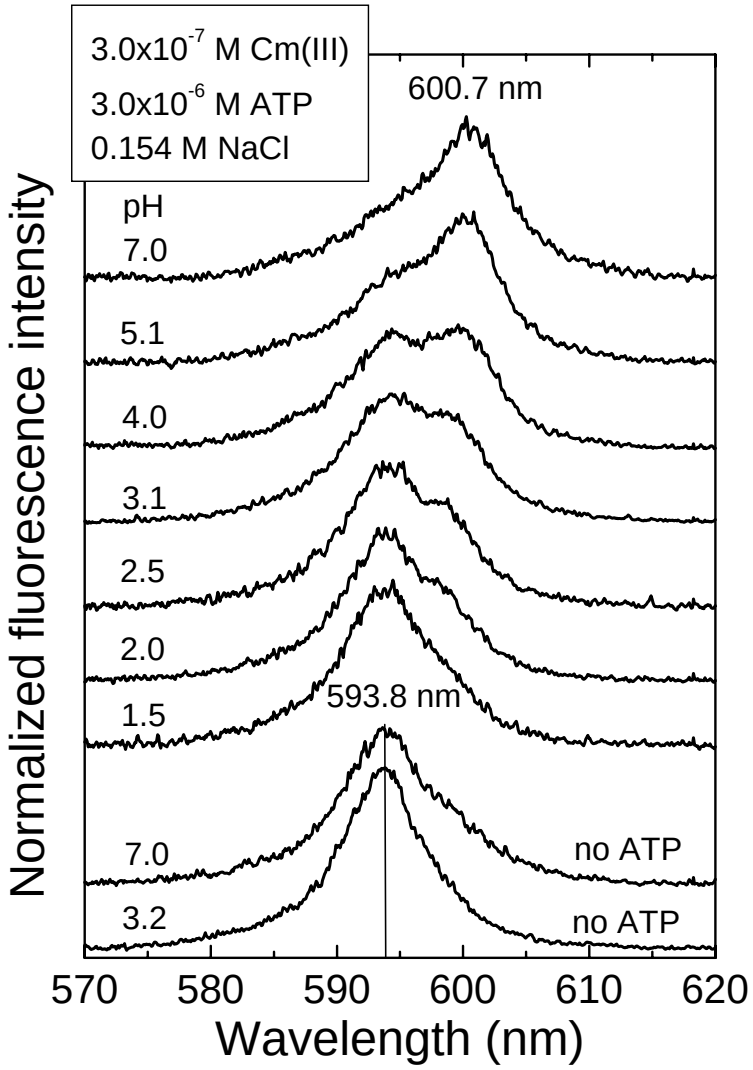

Fig. 3.2.4: Fluorescence emission spectra of $3x10^{-7}$ M Cm(III) in 0.154 M NaCl solution containing $3x10^{-6}$ M ATP at various pH; the spectra are scaled to the same peak area.

When adding ATP and changing the pH to 7.0, there is a pronounced red-shift of the emission, 6.9 nm, as a result of the complex formation. In another series of samples at pH 4.5 the measurements revealed one Cm(III) peak with a maximum at 600.4 nm at ATP concentrations above $3x10^{-6}$ M. At pH 6.5 the peak maximum is shifted to 601.8 nm at ATP concentrations above $1.2x10^{-5}$ M. This might indicate the formation of different Cm-ATP species.

To describe the complex formation reactions in the system Cm(III)-ATP, we applied the factor analysis program code SPECFIT [62]. Input parameters for the data fitting were the known total concentrations of Cm^{3+}, ATP, the pH of each sample, and the protonation constants for ATP published in [63]. As a result, we could develop a chemical model describing the ongoing processes in the Cm(III)-ATP system. It could be demonstrated that predominantly 1:1 complexes of the type $M_pH_qL_r$ were formed under the given experimental conditions [38]. The dependencies found in the TRLFS data could be expressed by the following equilibria:

$$Cm^{3+} + ATP^{4-} + 2H^{+} \leftrightarrow CmH_2ATP^{+} \quad (1)$$

$$Cm^{3+} + ATP^{4-} + H^{+} \leftrightarrow CmHATP \quad (2)$$

$$Cm^{3+} + ATP^{4-} \leftrightarrow CmATP^{-} \quad (3)$$

Formation constants for reactions (1) to (3) were calculated to be log $ß_{121}$ = 16.86 ± 0.09, log $ß_{111}$ = 13.23 ± 0.10 and log $ß_{101}$ = 8.19 ± 0.16, respectively. In test solutions with an excess of ATP greater than 1:500 the TRLFS spectra give evidence for the existence of a further Cm-ATP species, presumably a 1:2 complex.

Figure 3.2.5 shows a comparison of the single component spectra obtained in the Cm-ATP and the Cm-*D.äspöensis* system.

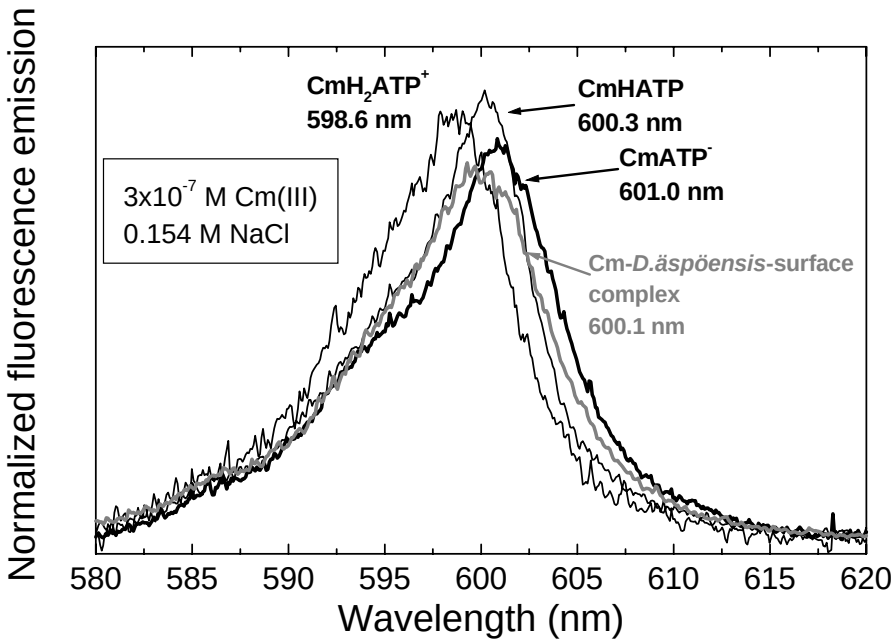

Fig. 3.2.5: Fluorescence emission spectra of CmH_2ATP^{+}, CmHATP, $CmATP^{-}$ and Cm-*D. äspöensis*-surface complex as derived by peak deconvolution; the spectra are scaled to the same peak area.

The shape of the spectrum and the peak maximum, 600.1 nm, of the sorbed Cm(III) on the cell envelope of *D. äspöensis* show a good agreement with those of the Cm-ATP species (see Figure 3.2.5). Moreover, the fluorescence emission lifetime of the Cm(III)-*D.äspöensis*-surface complex of 162±5 µs lies in the same range like the lifetime of $CmATP^-$, 187±7 µs. In both cases only approximately three water molecules remain in the first coordination sphere. These results support the conclusions drawn in paragraph 3.2.2 and in [44] for a favored interaction of Cm(III) with organic phosphato-groups of the cell envelope of *D. äspöensis*. Anyhow, for a detailed explanation of the binding mechanism, more investigations of many different model compounds are still necessary.

3.3 Interaction with neptunium(V)

The goal of this part of the project is to explore interaction processes of the SRB *D. äspöensis* with pentavalent actinides. As representative for pentavalent actinides neptunium, NpO_2^+, was chosen. In general less is known about bacterial interactions of Np(V) with microorganisms. Moreover, Np(V) complexes ligands poorly and is thought to be non-sorptive. Only one paper so far, describes the biosorption of NpO_2^+ by *Pseudomonas fluorescens* [64]. At $[Np(V)]_{initial}$ of $4.75x10^{-6}$ M and biomass concentrations >0.93 g/l, 85% of Np(V) was sorbed under aerobic conditions at pH 7 within 15 min. The biosorption increased with pH from 6 to 8.
The other contributions in the literature are describing the process between mixed cultures and Np(V). In [65] a removal of Np(V) by a combination of two microbial processes: a) bio-reduction to Np(IV) by *Shewanella putrefaciens* followed by b) a bio-precipitation by *Citrobacter* sp. (phosphate liberation) is described. An anaerobic, sulfate-reducing consortium (identified strains: *D. desulfuricans* A, *D. desulfuricans* B, *D. gigas* and a strain closely resembling *D. vulgaris*) reduced Np(V) to Np(IV) with precipitation of a Np(IV) solid (but only growing cultures) [66].

3.3.1 Experimental

The bacteria were grown and characterized as described in chapter 2. The collected biomass was 0.95 ± 0.25 $g_{dry\ weight}$/l. A 0.033 M stock solution of $^{237}Np(V)$ in 0.1 M HNO_3 was used. The pentavalent oxidation state of Np was verified by near infrared (NIR) absorption spectroscopy. 1 ml of biomass suspension and 5 ml of Np(V) working solution were combined and gently shaken at 25°C under anaerobic conditions. Samples were taken after defined time steps. The separation of cells and supernatant solution was performed by centrifugation. The Np amount of the fractions was analyzed using ICP-MS and NIR spectroscopy. The medium contains Np(V) and 0.01 M lactate in 0.154 M NaCl. The pH was varied between 6 and 8. The experiments were performed at two different $[Np(V)]_{initial}$ of $1x10^{-4}$ and $1x10^{-5}$ M. In one set of experiments Np(V) and U(VI) were simultaneously provided.
The Np(V) speciation in the starting solutions is dominated by (ca. 64%) NpO_2^+ and (ca. 36%) the lactate complex NpO_2(HLAC) .

3.3.2 Results and discussion

In this project, we could show for the first time the removal of Np(V) from the solution by cells of *D. äspöensis*. In all samples where no cells were added, the Np concentrations measured by ICP-MS did not differ significantly from the initial values. Figure 3.3.1 shows the results of the time dependent decrease of Np and U in the presence and absence of biomass at $[Np, U]_{initial}$ of $1x10^{-5}$ M and at pH 6.

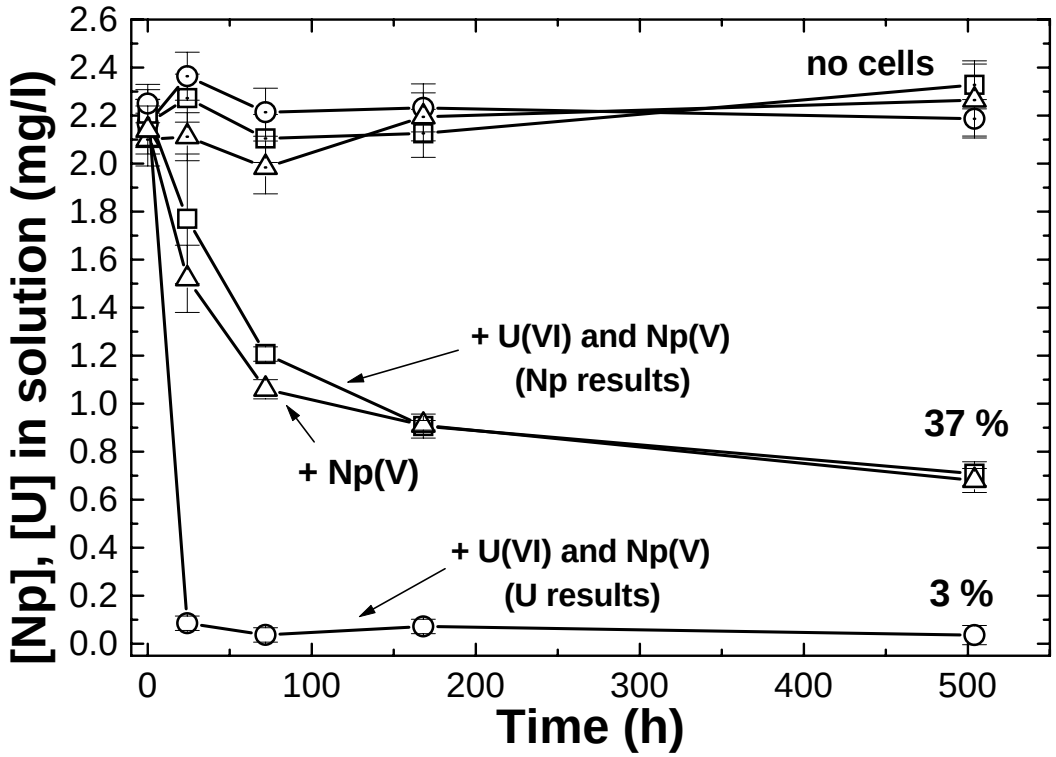

Fig. 3.3.1: Decrease of the U(VI) and Np(V) concentration ($[U(VI)]_{initial}$: 2.25 mg/l, $[Np(V)]_{initial}$: 2.21 mg/l) in solution in dependence of the contact time.

The main Np(V) removal occurred after the first 72 h. After 168 h, limiting values are reached. In contrast to these results, uranium interacts with the biomass in a faster way. Furthermore, we observed a stronger interaction of U(VI) with the biomass compared to Np(V). Interestingly, we found no difference in the amount of accumulated Np(V) by the biomass in the presence or the absence of U(VI) in the test solutions. This might indicate the occurrence of different binding sites and/or binding modes for Np and U on the cell envelope of *D. äspöensis*. From the time dependence shown in Figure 3.3.1 one might conclude that probably two different processes occur after adding the biomass.

The pH is another factor which limits the Np removal efficiency. A slight increase from 63 to 77% was observed when the pH changed from 5.95 to 7.70, respectively (Figure 3.3.2).

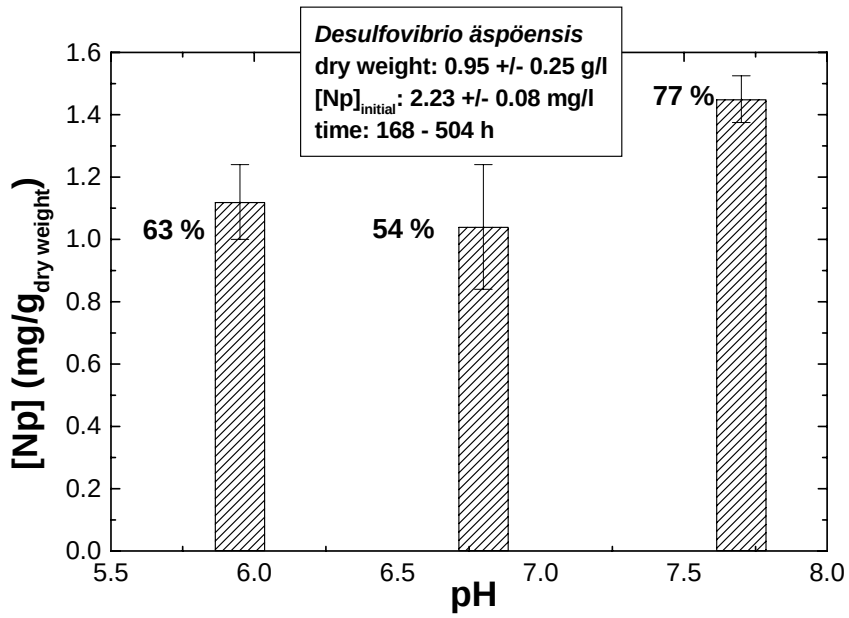

Fig. 3.3.2: Total amount of Np(V) removed from the solution by *D. äspöensis* as a function of pH.

Almost no Np(V) was bound to the biomass at $[Np(V)]_{initial}$ of 23.7 mg/l at pH 3 and pH 5.

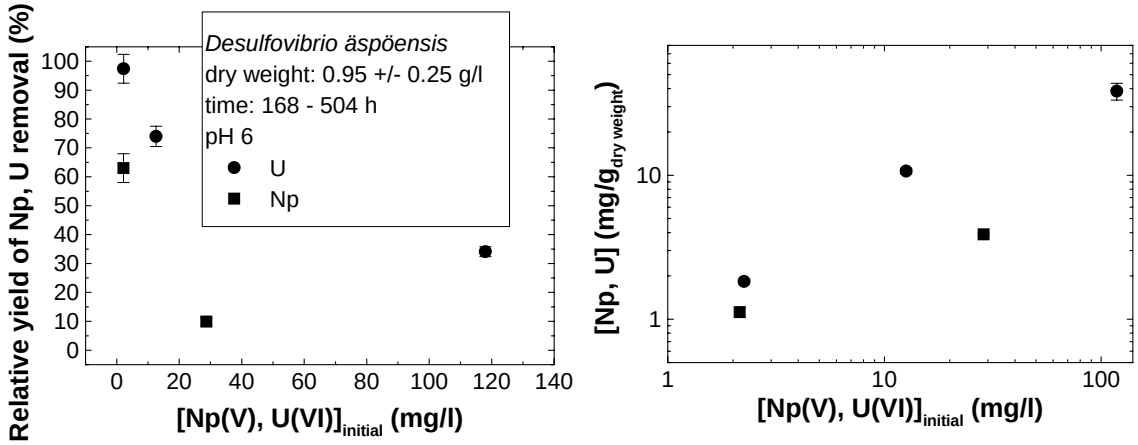

Fig. 3.3.3: Removed neptunium/uranium from the solution in the presence of *D. äspöensis* at pH 6.

Besides the pH, the Np concentration in solution also limits the removal efficiency (Figure 3.3.3). Only at low $[Np(V)]_{initial}$, 2.15 mg/l, a removal efficiency above 50%, 63 % (1.21

mg/$g_{dry\ weight}$), could be achieved. Whereas, at $[Np(VI)]_{initial}$ of 28.68 mg/l, the removal efficiency decreased to a level of 9.9 % (3.89 mg/$g_{dry\ weight}$).

Unfortunately up to now, we have no experimental proof for the formation of Np(IV) due to the activity of the cells. NIR measurements of the bacterial suspensions and the supernatants showed only small differences in the intensity of the absorption band at 981 nm. Thus more than 90 % of the Np occurs as Np(V). This point to the fact that the determination of the speciation of the bound Np, e.g., by NIR spectroscopy, is difficult due to the low amount of Np associated with the biomass.

This study gives further proofs for the weak sorption and complexation properties of Np(V). The experiments performed with Pu, which will be presented in the next chapter, are in agreement with those obtained for Np(V). More than 75 % of the Pu(V) was found in solution due to the weak complexation ability of the PuO_2^+ ion.

3.4 Interaction with plutonium

The aim of this part of the project is to explore the interaction processes of the SRB *D. äspöensis* with plutonium. Characteristic for Pu is that this element can exhibit several oxidation states, e.g., +4, +5, and +6, in aqueous solution under environmental conditions [67]. Most of the papers on interactions of Pu with microbes are reporting only data on the amount of accumulated plutonium by the biomass without providing information on the ongoing processes [68-70]. In [71], a first attempt was made to determine the reduction products of Pu(IV) after contact with iron-reducing bacteria. Metabolically active cells of *Microbacterium flavescens* are able to take up siderophor complexes of Pu(IV) [72]. Papers reporting the interaction processes of Pu(VI) with microbes are rare. Hexavalent plutonium has a high solubility and is relatively stable compared to Pu(IV) under aerobic conditions. Thus Pu(VI) has a high potential of migration away from nuclear waste repositories. Panak and Nitsche are giving an excellent overview about bacterial interactions of Pu(VI) with the soil bacteria *Pseudomonas stutzeri* ATCC 17588 and *Bacillus sphaericus* ATCC 14577 [55]. One third of the initially present Pu(VI) was reduced to Pu(V) after 24 h. After one month also 16% of Pu(IV) was formed. The Pu(IV) was not produced by microbial reduction. It is rather a result of the disproportionation of the formed Pu(V) or autoreduction of Pu(VI). The over all process is divided into three parts: a) complexation of Pu(VI) with phosphate groups of the cell surface, b) reduction of Pu(VI) to Pu(V) and dissolution of Pu(V), and c) disproportionation of Pu(V) to Pu(IV) and Pu(VI) and complexation of Pu(IV) with the biomass.

On the following pages, we are describing the interaction of Pu with cells of *D. äspöensis*. The Pu was provided in two oxidation states namely ca. 46% as Pu(VI) and ca. 34% as Pu(IV)-polymer.

3.4.1 Experimental

Preparation of the ^{242}Pu stock solution

The starting compound was a green-brown powder of PuO_2 (AEA technology QSA GmbH) with the following composition: 0.009% of Pu-238, 0.008% Pu-239, 0.020% Pu-240, 0.017% Pu-241, 99.945% Pu-242, and 0.001% Pu-244. The problem is that this substance is chemically highly inert and dissolves extremely slowly in acids [73]. In a first step, a certain amount of the oxide was mixed with 15 ml of 4.3 M HNO_3. The Pu suspension was boiled under reflux. After a reaction time of 2265 min a dark-green solution of 0.0165 M Pu(IV) was obtained. This solution contained besides the Pu(IV) also Pu(IV)-polymers. The solution was separated from the PuO_2 particles by centrifugation. In the next step, we tried to synthesize a Pu(III) stock solution from the Pu raw solution by electrolysis.

Fig. 3.4.1: Image of the electrolysis cell in the glove box. Cathode-chamber: Pu raw-solution, Anode-chamber: 2 M $HClO_4$.

The reason for preparing a Pu(III) stock solution was that this oxidation state is less effected by disproportionation reactions and colloid formation. First, the formation of nitrous gases was observed showing the decomposition of nitrate. However, we failed in preparing a Pu(III) stock solution probably due to the presence of nitrate at low concentrations and Pu(IV)-polymers which could not be decomposed by the electrolysis. The Pu was then precipitated as $Pu(OH)_4$ by adding stepwise 5 M NaOH. The precipitate was washed twice with 0.01 M NaOH and dissolved in 2.2 M $HClO_4$. This solution was again electrolyzed to obtain a Pu(VI) stock solution. The UV-VIS-NIR spectra of the Pu(VI) stock solution obtained after different electrolysis times are summarized in Figure 3.4.2.

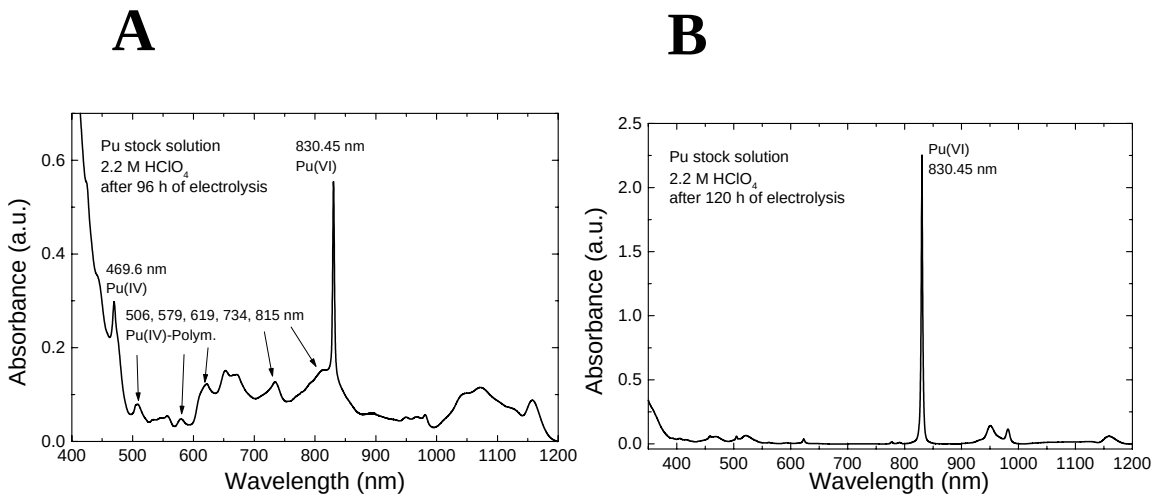

Fig. 3.4.2: Absorption spectra of the Pu stock solution ([^{242}Pu] 5.35x10^{-3} M) in 2 M $HClO_4$. A) after 96 h electrolysis and B) after 120 h electrolysis.

The characteristic absorption bands (the wavelength and band shape) of the different Pu oxidation states were identified according to [73]. After an electrolysis time of 96 h the absorption bands of Pu(IV), Pu(IV)-polymers and Pu(VI) can be localized. After 120 h only the absorption bands of Pu(VI) are visible. Before preparing the Pu working solutions for every experiment, the Pu stock solution was shortly electrolyzed to obtain a maximum on Pu(VI).

Because of the low absorption coefficients of Pu(IV), Pu(V), and Pu(IV)-polymer [73] and the low concentration of Pu in solution, the quantification of the different oxidation states of Pu was performed by liquid-liquid-extraction. As extracting agents 2-Theonyltrifluoroacetone (TTA, 0.5M) in xylene, and Phosphoric acid bis-(2-ethyl-hexyl)ester (HDEHP, 0.5M) in toluene were taken according to [74, 75]. With TTA at pH 0 the Pu(IV) state is extracted in the organic phase, Pu(III), (V), (VI) and Pu(IV)-polymers remain in the aquatic phase. With HDEHP at pH 0 the Pu(IV)- and Pu(VI)-state are extracted in the organic phase and Pu(III), (V), and Pu(IV)-polymers remain in the aquatic phase. Using HDEHP at pH 1 Pu(III), (IV), and (VI) are extracted in the organic phase whereas Pu(V), and Pu(IV)-polymers remain in the aquatic phase. Extraction of a $Cr_2O_7^{2-}$ (0.021M) oxidized solution with HDEHP at pH 0 leaves only the Pu(IV) polymeric species in the aqueous phase, whereas Pu(III), (IV), (V), and (VI) are extracted in the organic phase.

All plutonium concentrations were measured by liquid scintillation counting (LSC) using a LS counter, Wallac system 1414 (Perkin Elmer). For this, defined volumes (0.1 to 1 ml) of the samples were mixed with 15 ml of a Ultima Gold scintillation cocktail.

Table 3.4.1 summarizes the results of the liquid-liquid-extraction of the Pu stock solution after electrolysis.

Tab. 3.4.1: Results of the liquid-liquid-extraction of the ^{242}Pu stock solution.

Percentage	Pu stock solution
Pu(IV)	0.98±0.05
Pu(VI)	71.3±6.0
Pu(III)	7.0±0.7
Pu(V)	0
Pu(IV)-polymer	20.7±2.1
Recovered	97.6±4.2

As depicted in Table 3.4.1, the Pu stock solution still contained, besides approximately 70% Pu(VI), approximately 21% Pu(IV)-polymers due to the synthesis procedure.

Experiments with the bacteria

The bacteria were grown and characterized as described in chapter 2. The collected biomass was 0.83 ± 0.15 $g_{dry\ weight}$/l. 0.25 ml of biomass suspension and 1.25 ml of Pu working solution were combined and gently shaken at 25°C under anaerobic conditions. Samples were taken after defined time steps. The separation of cells and supernatant solution was performed by centrifugation. The Pu present in the different fractions was analyzed using UV-VIS-NIR spectroscopy, liquid-liquid-extraction, and LSC. For the extractions 0.5 ml of the respective fraction was extracted with 1 ml of the extracting agent. Experiments were performed at pH 5 at varying $[^{242}Pu]_{initial}$ between 7.6 and 254 mg/l. Detailed investigations of the distribution of the different oxidation states of Pu were made at a fixed concentration of Pu, $[^{242}Pu]_{initial}$ of 14.9 ± 1.10 mg/l, with and without 0.01 M lactate.

3.4.2 Results and discussion

In a first series of experiments, we investigated the amount of accumulated plutonium depended on the interaction time and as a function of the $[^{242}Pu]_{initial}$.

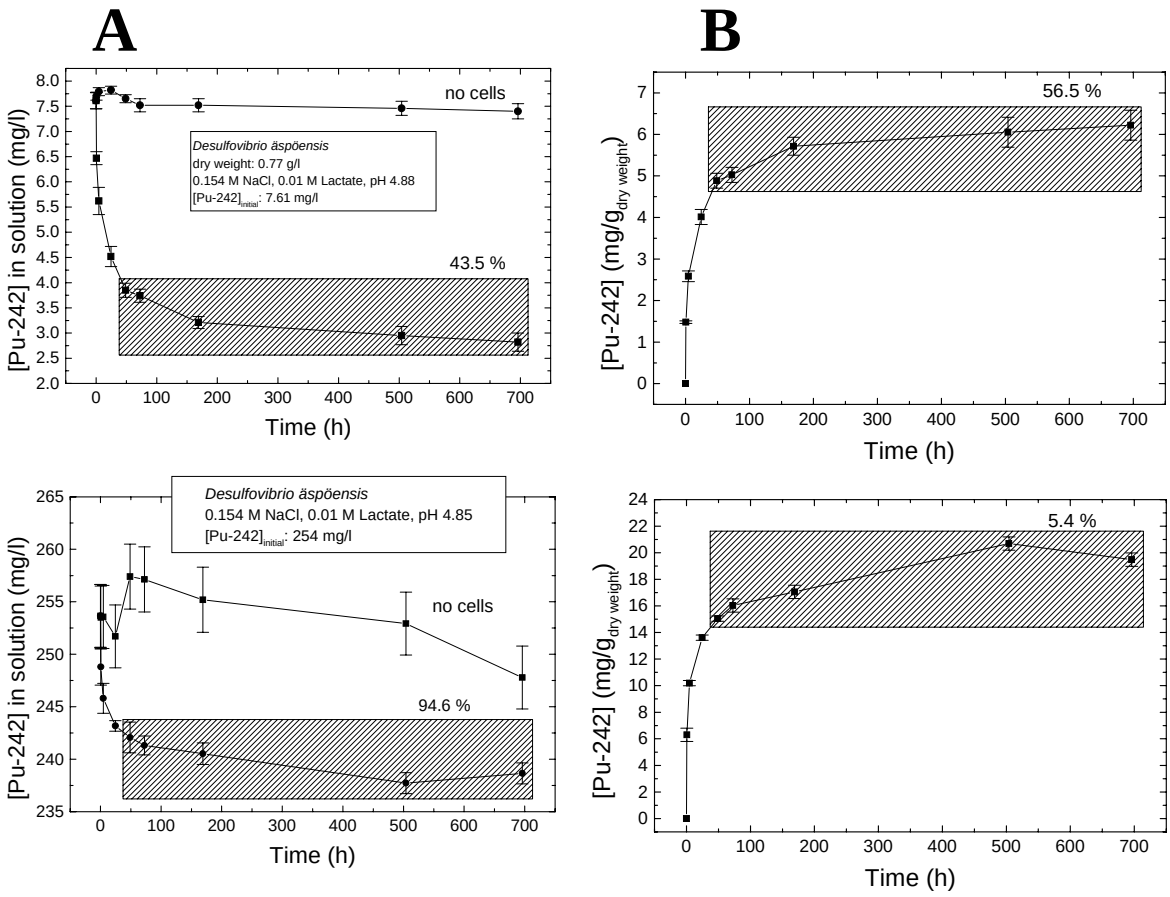

Fig. 3.4.3: (A) Decrease of the ^{242}Pu concentration in solution and (B) Increase of the amount of accumulated ^{242}Pu by the cells of *D. äspöensis* at two different concentrations of $[^{242}Pu]_{initial}$.

Figure 3.4.3 shows the decrease of the ^{242}Pu concentration in solution with increasing contact time at two $[^{242}Pu]_{initial}$: 7.61 mg/l and 254 mg/l. The increased amount of ^{242}Pu associated with the biomass is also shown. The main Pu removal occurred after the first 24 h, whereas limiting values were achieved after 72 h. The time dependence depicted in Figure 3.4.3 indicates again an overall process consisting of at least two different steps. We have noticed the close similarities between the U- and the Pu-*D. äspöensis*-system. In agreement with the U(VI) and the Np(V) results, we have found again a strong dependence of the amount of Pu associated with cells of *D. äspöensis* from the initial concentration of ^{242}Pu in the test

solutions. In Figure 3.4.4, we are comparing the results obtained in the U(VI) system with those of the ^{242}Pu system.

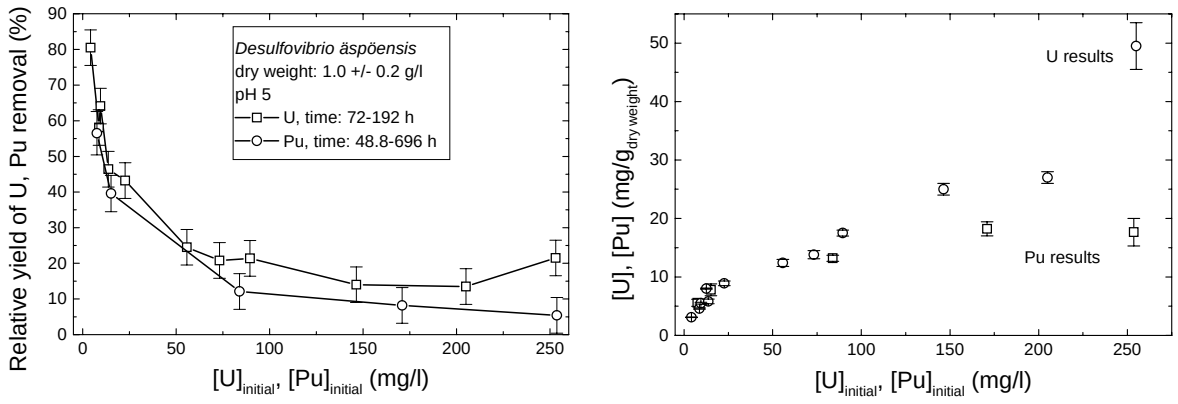

Fig. 3.4.4: Removed uranium and plutonium from the test solutions by cells of *D. äspöensis* as a function of the initial actinide concentration at pH 5.

At initial Pu concentrations ranging from 7.6 to 15.2 mg/l, we observed removal efficiencies of 56 and 40%. Whereas at $[^{242}Pu]_{initial}$ > 83 mg/l, the removal efficiency decreased to a level of 12 and finally to 5.4%. Comparing the plutonium results with uranium, the measurements indicate that the cells of *D. äspöensis* accumulating less plutonium. The decreased amount of accumulated plutonium with increasing initial Pu concentrations points to the effect of toxicity and metal stress to the cells caused by plutonium. Compared to uranium this effect is even stronger in the case of plutonium. This could be explained by an increased toxicity/radiotoxicity of ^{242}Pu towards *D. äspöensis* compared to U. With increasing $[^{242}Pu]_{initial}$, we observed a slower increase of the total amounts of associated Pu on the biomass compared to U. The maximum concentration was 18 ± 2 $mg/g_{dry\ weight}$.

In this first set of experiments, two liquid-liquid-extractions were applied, a) 0.5 M TTA in xylene at pH 0 and b) 0.5 M HDEHP in toluene at pH 0. With these extractions one can distinguish between Pu(IV), Pu(VI) and a fraction containing Pu(III), Pu(V) and Pu(IV)-polymers [74]. The following samples were analyzed: a) the blanks without biomass, b) the Pu solution separated from the biomass (supernatant) and c) the biomass suspension in 1 M $HClO_4$ after washing with 0.9% NaCl at pH 5. The extractions were performed after a contact time of 696 h. To determine the oxidation state distribution of Pu bound to the biomass, the cell suspensions were acidified to pH 0 to remove the Pu from the biomass [50]. After an interaction time of 1 h the liquid-liquid-extraction was done. The centrifugation experiments showed an incomplete dissolution of the cells in 1 M $HClO_4$ after 1 h. Moreover, the results of this set of samples revealed that only 38 to 58% of the total amount of the bound Pu could

be removed from the cells. This shows that 42 to 62% of the accumulated Pu is relatively strongly bound to the biomass after 696 h. The results of the oxidation state determinations are summarized in Table 3.4.2.

Tab. 3.4.2: Pu oxidation state distribution in experiment 1 after an interaction time of 696 h.

Percentage	Blanks (no biomass)	Separated Pu solution after interaction	Washed biomass and suspended in 1 M $HClO_4$
Pu(IV)	0.40±0.5	1.00±1.2	6.70±2.5
Pu(VI)	3.40±2.0	3.80±2.9	7.00±1.6
Pu(III), Pu(V), Pu(IV)-polymer	89.70±2.3	88.60±2.9	25.40±5.2
Recovered	92.3±0.6	91.3±2.4	40.4±4.3
% of Pu not extractable (strongly bound)			59.6±4.3

No differences in the Pu oxidation state distribution were observed depended on the initial Pu concentration present in the test solutions. Table 3.4.2 depicts the average values of all Pu initial concentrations investigated. Only 40% of the associated Pu could be extracted. An increased amount of Pu(IV) and Pu(VI) bound to the biomass was identified compared to the supernatant and the blank samples. The largest amount of the accumulated Pu belongs to the fraction containing Pu(III), Pu(V), and Pu(IV)-polymer. The data summarized in Table 3.4.2 are not sufficient to describe the interaction process of Pu with *D. äspöensis* in detail. Further experiments were performed with and without lactate and oxidation state distribution determinations after 24, 72, 168, and 720 h which will be described below.

In the following experiments, the $[^{242}Pu]_{initial}$ was fixed to 14.8 ± 0.82 mg/l and the biomass concentration varied between 0.90 ± 0.20 g/l.

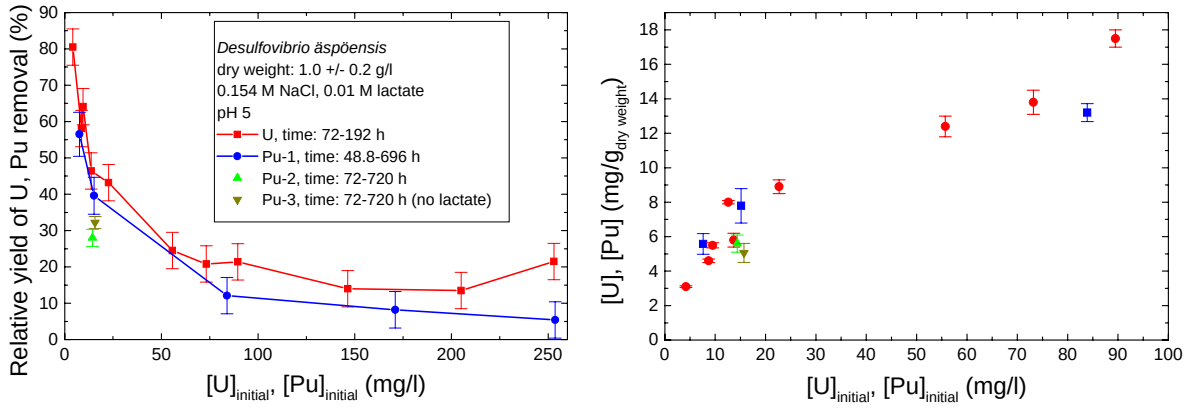

Fig. 3.4.5: Summary of the removed uranium and plutonium from the test solutions by cells of *D. äspöensis* as a function of $[U, Pu]_{initial}$ at pH 5.

The parameters measured at $[Pu]_{initial}$ 15.1 ± 0.7 mg/l in the three different Pu experiments; a) remaining Pu in solution: 10.0 ± 0.9 mg/l, and b) Pu bound to the cells: 6.20 ± 1.6 $mg/g_{dry\ weight}$; are in relative good agreement (see Figure 3.4.5).

Pu speciation in the blank solutions

The measured absorption spectra of the blank solutions 1 containing 0.01 M lactate are summarized in Figure 3.4.6.

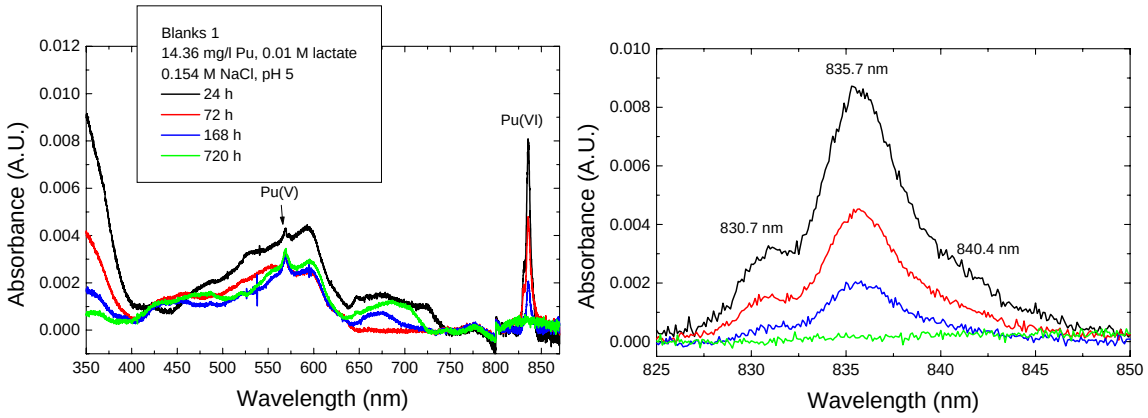

Fig. 3.4.6: Absorption spectra of the blank solutions 1 in dependence of the time ([^{242}Pu]: 14.36 mg/l, 0.01 M lactate, 0.154 M NaCl, pH 5).

Two oxidation states of the Pu can be identified according to [73], Pu(V) at approximately 568 nm and Pu(VI) in the wavelength range 825 to 850 nm. Interestingly, we found a reduction of Pu(VI) already due to the presence of 0.01 M lactate in the test solutions. The absorption band of Pu(VI) is decreasing with the increasing reaction time. The observations of the absorption spectra are in agreement with the results of the liquid-liquid-extractions.

Tab. 3.4.3: Pu oxidation state distribution measured in the lactate containing blank solutions.

Percentage	24 h	72 h	168 h	720h
Pu(IV)	0.60	0.20	0.10	0.15
Pu(VI)	22.7±5.3	15.3±6	7.3±2.7	0.90
Pu(III)	n.d.	n.d.	n.d.	2.67
Pu(V)	n.d.	n.d.	n.d.	54.8±11
Pu(IV)-polymer	n.d.	n.d.	n.d.	32.6
Pu(III), Pu(V), Pu(IV)-polymer	65.3±5.3	73.0±6	77.5±2.7	90.1
Recovered	84.8±5.3	84±6	83±2.6	90.4±9.0

The absorption spectra of Pu(VI) showed in Figure 3.4.6 exhibit characteristic changes in the position and the shape of the absorption bands compared to a Pu(VI) solution without lactate

(see Figure 3.4.8). Similar changes were observed by Eberle et al. [76] in the Pu(VI)-glycolate system. Therefore, we attribute these observations to a complexation of Pu(VI) by lactate. To the knowledge of the authors, complex formation constants of Pu(VI) with lactate are not reported in the literature. The measured absorption spectra represent the sum of the absorption signals of the uncomplexed PuO_2^{2+} ion (830.7 nm), the $PuO_2(LAC)^+$ complex (835.7 nm) and the $PuO_2(LAC)_2$ complex (840.4 nm). As a comparison, the absorption bands for the glycolate species were determined to be: 835.4 nm for $PuO_2(GLY)^+$ and 839.6 nm for $PuO_2(GLY)_2$ [76]. The spectra were deconvoluted into single peaks for the three species in order to determine their concentration. Figure 3.4.7 shows a measured absorption spectrum of a Pu solution with lactate and its deconvolution. For an estimate of the formation constants in the Pu(VI)-lactate system the assumptions were made that the complexes of Pu(VI) with OH^- and Cl^- have only minor influence and the complexation of lactate with Pu in the other minor oxidation states can be neglected.

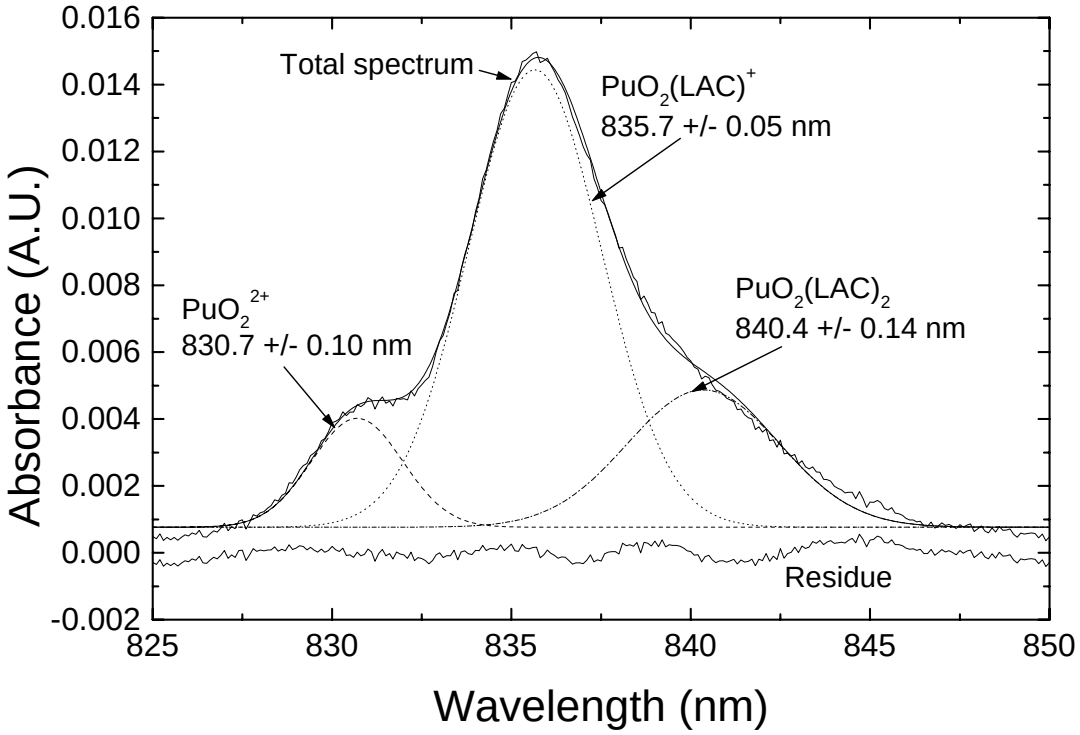

Fig. 3.4.7: Absorption spectrum of Pu(VI) in lactate solution and its deconvoluted absorption bands ([LAC]: 0.012 M, $[PuO_2^{2+}]$: 2.27×10^{-5} M, pH 5, 0.154 M NaCl).

The species concentrations were calculated based on the results from the peak deconvolution of the sum spectra.

The following complex formation reactions were postulated:

$$PuO_2^{2+} + LAC^- \leftrightarrow PuO_2(LAC)^+ \quad (1)$$

$$PuO_2^{2+} + 2LAC^- \leftrightarrow PuO_2(LAC)_2 \quad (2)$$

Formation constants for reactions (1) and (2) were calculated to be log $ß_{PuO2(LAC)+}$ = 2.75 ± 0.09 and log $ß_{PuO2(LAC)2}$ = 4.22 ± 0.10, respectively. Table 3.4.4 shows a comparison of the complex formation constants determined in the Pu(VI), U(VI) lactate and glycolate systems.

Tab. 3.4.4: Relevant stability constants of glycolate (GLY) and lactate (LAC) complexes of Pu(VI) and U(VI).

Complex	Method	log β	T (°C)	I (M)	Reference
$UO_2(GLY)^+$	Potentiometry	2.38 ± 0.01	20	1.0 ($NaClO_4$)	Magon et al. [77]
	UV-vis	2.32 ± 0.16	22		Moll et al. [78]
	TRLFS	2.52 ± 0.20			
$UO_2(GLY)_2$	Potentiometry	3.95 ± 0.04	20		Magon et al. [77]
$PuO_2(GLY)^+$	UV-vis-NIR	2.43 ± 0.08	25	($NaClO_4$)	Eberle et al. [76]
	Potentiometry	2.16 ± 0.01	22	($NaClO_4$)	Magon et al. [77]
$PuO_2(GLY)_2$	UV-vis-NIR	3.79 ± 0.17	25	($NaClO_4$)	Eberle et al. [76]
	Potentiometry	3.45 ± 0.04	22	1.0 ($NaClO_4$)	Magon et al. [77]
$UO_2(LAC)^+$	Potentiometry	2.77 ± 0.01	20	1.0 ($NaClO_4$)	Magon et al. [77]
$UO_2(LAC)_2$		4.52 ± 0.04			
$PuO_2(LAC)^+$	UV-Vis-NIR	2.75 ± 0.06	25	0.154 (NaCl)	this work
$PuO_2(LAC)_2$		4.22 ± 0.10			

The summary of relevant formation constants for U(VI) and Pu(VI) complexes with glycolate and lactate showed that the UV-VIS-NIR data evaluation results in reasonable stability constants. In [76] and [77] the same trend, a decrease of the complex stability from U(VI) to Pu(VI) was observed.

To summarize, the Pu(VI) speciation in the lactate containing test solutions consists of 11.7±2.1% PuO_2^{2+}, 67.8±2.3% $PuO_2(LAC)^+$, and 20.5±0.6% $PuO_2(LAC)_2$.

Figure 3.4.8 shows the time dependence of the absorption spectra of the Pu working solution without lactate before adding the cells.

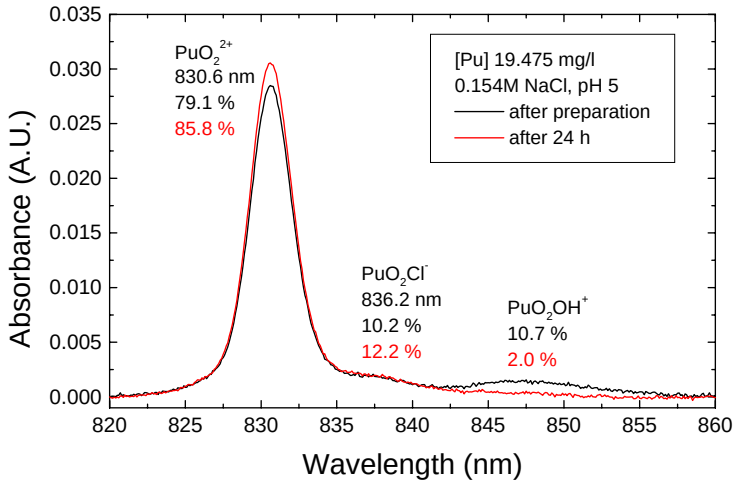

Fig. 3.4.8: Absorption spectrum of the Pu working solution ([^{242}Pu] = 19.475 mg/l, 0.154 M NaCl, pH 5) at two different times after preparation.

Speciation calculations using the formation constants for the Pu(VI) hydroxide and chloride species published in [79] showed that 14% of the Pu(VI) exist as $PuO_2(OH)^+$ and 14% occur as PuO_2Cl^- at pH 5. The absorption spectrum measured shortly after sample preparation is in agreement with the speciation calculation. After 24 h we observed a decrease of the absorption band of the PuO_2OH^+ complex accompanied by an increase of the intensity of the PuO_2^{2+} absorption band. At the moment, this effect is not fully understood.

The blank solutions 2 (see Figure 3.4.9) were prepared by taking appropriate volumes of the ^{242}Pu working solution shown in Figure 3.4.8.

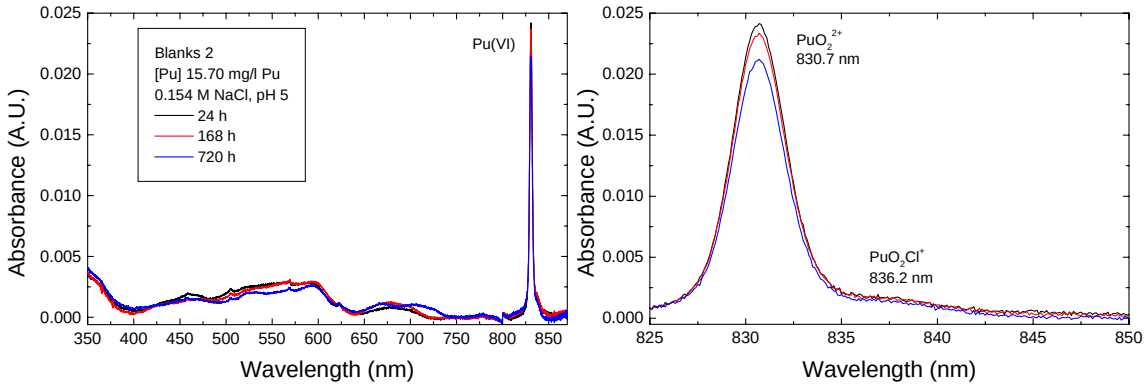

Fig. 3.4.9: Absorption spectra of the blank solutions 2 in dependence of the time ([^{242}Pu]: 15.59 mg/l, 0.154 M NaCl, pH 5).

One main oxidation state of Pu can be identified according to [73], Pu(VI) at 830.7 nm. Small indications were found for Pu(V) at 568 nm. Pu(VI) remains relatively stable under this conditions in solutions of 0.154 M NaCl at pH 5.
The results of the liquid-liquid-extractions of the blank solutions 2 are summarized in Table 3.4.5.

Tab. 3.4.5: Pu oxidation state distribution in the blank solutions 2.

Percentage	24 h	72 h	168 h	720h
Pu(IV)	0.22	0.23	0.19	0.15
Pu(VI)	46.9±15	46.8±14.8	46.6±13.8	39.2±10.4
Pu(III)	1.94±0.93	3.50±2.0	1.13±1.1	1.48±0.50
Pu(V)	5.50±6.3	5.50±6.5	8.90±5.9	20.9±4.4
Pu(IV)-polymer	31.7	31.8	32.3	26.5
Recovered	82.5±12.6	84.0±12.9	85.8±11.8	82.2±7.6

The liquid-liquid-extractions indicated that the main amount of the Pu consists of Pu(VI) and Pu(IV)-polymers. After 720 h of reaction time the amount of Pu(V) increased to about 21%.
To summarize, the Pu(VI) in the test solutions without lactate occurs as PuO_2^{2+} (87.2±1.6%) and PuO_2Cl^+ (12.6±1.4%).

^{242}Pu and Desulfovibrio äspöensis

In all test solutions with cells of *D. äspöensis*, a fast reduction of Pu(VI) to Pu(V) due to the activity of the biomass was observed. A summary of the liquid-liquid-extractions are given in Figure 3.4.10.

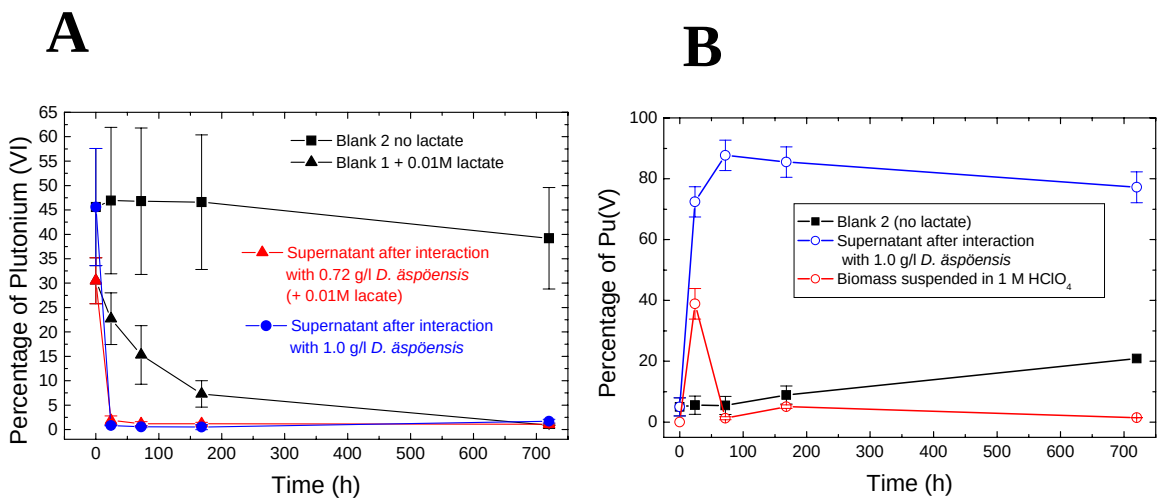

Fig. 3.4.10: A) Distribution of Pu(VI) and B) of Pu(V) identified in the different fractions by means of liquid-liquid-extraction.

As it can be seen in Figure 3.4.10, if cells of *D. äspöensis* are present then lactate has no influence on the decrease of Pu(VI) in the test solutions. Therefore, we are focusing the discussion of the Pu oxidation state distribution on the basis of the experiments without lactate. Table 3.4.6 gives an overview concerning the oxidation state distribution of Pu in the test solutions after separating the cells by centrifugation.

Tab. 3.4.6: Pu oxidation state distribution in the supernatant after separating the cells determined by means of liquid-liquid-extraction.

Percentage	24 h	72 h	168 h	720 h
Pu(IV)	0.10	0.15	0.22	0.65
Pu(VI)	0.83±0.08	0.56±0.18	0.52±0.55	1.72±0.4
Pu(III)	0.27	0.80	0.60	0.46
Pu(V)	72.4±5.0	87.7±5.0	85.5±5.4	77.2±5.1
Pu(IV)-polymer	20.8	10.39	10.33	10.65
Recovered	93.6±4.3	97.3±6.3	95.6±5.8	87.8±6.7

Already after a contact time of 24 h, the amount of Pu(VI) decreased from 47 to 0.8%, whereas the Pu(V) content increased from 5 to 72%. This indicates a fast reduction of Pu(VI) to Pu(V) due to the activity of the cells. Because of the weak complexing properties of the PuO_2^+ ion, around 80% of the Pu(V) was detected in solution. Similar observation were made by Panak et al. [55] in their investigations of the interaction of Pu(VI) with *Pseudomonas stutzeri* and *Bacillus sphaericus*. The amount of Pu(IV)-polymer decreased from 21% after 24 h to 10.5% after 72 h and is then independent from the contact time. This points to the effect of a biosorption of Pu(IV)-polymers onto the biomass. The amounts of Pu(IV) and Pu(VI) are slowly increasing to 0.65 and 1.72%, respectively after 720 h. This can be explained by a disproportionation of the Pu(V) dissolved from the cells after reduction of Pu(VI). Indications for the occurrence of Pu(V) and Pu(IV)-polymers were found in the absorption spectra (see Figure 3.4.11).

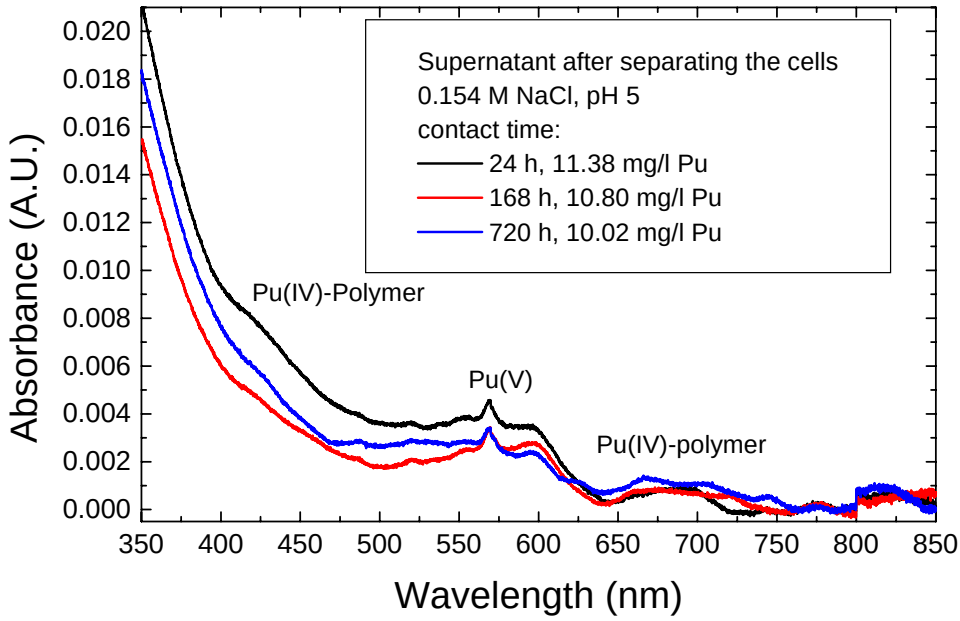

Fig. 3.4.11: Absorption spectra of the supernatant as a function of the contact time after separating the biomass by centrifugation.

After separating the supernatant from the cells, the bacteria were washed twice with 0.154 M NaCl at pH 5. The washed biomass was acidified to pH 0 by adding 1 M $HClO_4$. The aim of this procedure was a transfer of the biosorpt Pu from the biomass into the supernatant perchloric acid in order to determine the oxidation state distribution of the Pu associated with the cells (see Table 3.4.7).

Tab. 3.4.7: Pu amount in the acidified biomass suspension and in the supernatant perchloric acid after 1 h.

Contact time (h)	$[Pu\text{-}242]_{total}$ (mg/l) Biomass suspension in 1M $HClO_4$	[Pu] (mg/l) dissolved after 1 h	[Pu] (%) strongly bound
24	3.503±0.086	2.802 (80.0%)	20.0
72	3.390±0.022	2.520 (74.3%)	25.7
168	3.947±0.011	2.635 (66.8%)	33.2
720	4.847±0.066	2.298 (47.4%)	52.6

The results summarized in Table 3.4.7 indicate that always a certain amount of the accumulated Pu remains with the biomass. This amount of strongly bound plutonium increased from 20 to 53% after a contact time of 720 h. Therefore, the liquid-liquid-extractions were performed with the acidified biomass suspensions. The increase of the strongly bound Pu correlates with the recovered Pu of the extraction experiments (see Table 3.4.8).

Tab. 3.4.8: Oxidation state distribution of the Pu associated with the biomass.

Percentage	24 h	72 h	168 h	720 h
Pu(IV)	0.28	0.71	1.10	1.40
Pu(VI)	4.22±0.66	1.03±0.30	2.70±1.7	2.20±0.4
Pu(III)	35.4±5.0	10.2±1.0	3.70±1.0	13.60±12.8
Pu(V)	38.9±5	1.30±0.5	5.10±0.6	1.46
Pu(IV)-polymer	9.57	68.99	65.40	49.10
Recovered	88.3±2.0	80.5±2.4	77.4±1.0	62.5±9.9

After 24 h the amount of Pu(VI) was determined to be approximately 4.2%. This shows the biosorption and fast reduction of Pu(VI) to Pu(V). The later was measured to be 39%. This fast reduction is accompanied by a dissolution of the formed Pu(V) from the biomass as noticed above. The increased concentration of the Pu(IV)-polymers accumulated by the biomass, 9.6% after 24 h to 65.4% after 168 h, shows the interaction of Pu(IV)-polymers with the cells. We interpret the decreased amount of Pu(VI)-polymers from 168 to 720 h with an

accumulation inside the bacterial cells. Due to the toxicity of Pu towards *D. äspöensis* the cell envelope gets damaged as observed for uranium and Pu-species could penetrate inside the cells. The time dependent increase of the Pu(IV) concentration could be explained by a slow reduction process of Pu(V) to Pu(IV) which is from minor importance. Because the amount of Pu(IV) could be as well explained by a biosorption process of Pu(IV) which is formed by the disproportionation reaction of the dissolved Pu(V). However, a bioreduction to Pu(IV) followed by formation of Pu(IV)-polymers is also imaginable. Between 72 and 720 h of contact time, we observed an increase of the Pu(VI) concentration from 1 to 2.2 %. The origin of the biosorpt Pu(VI) is probably the disproportionation process of the dissolved Pu(V).
On the basis of our results and taking into the consideration the work of Panak et al. [55], we developed a model which describes the ongoing processes (see Figure 3.4.12).

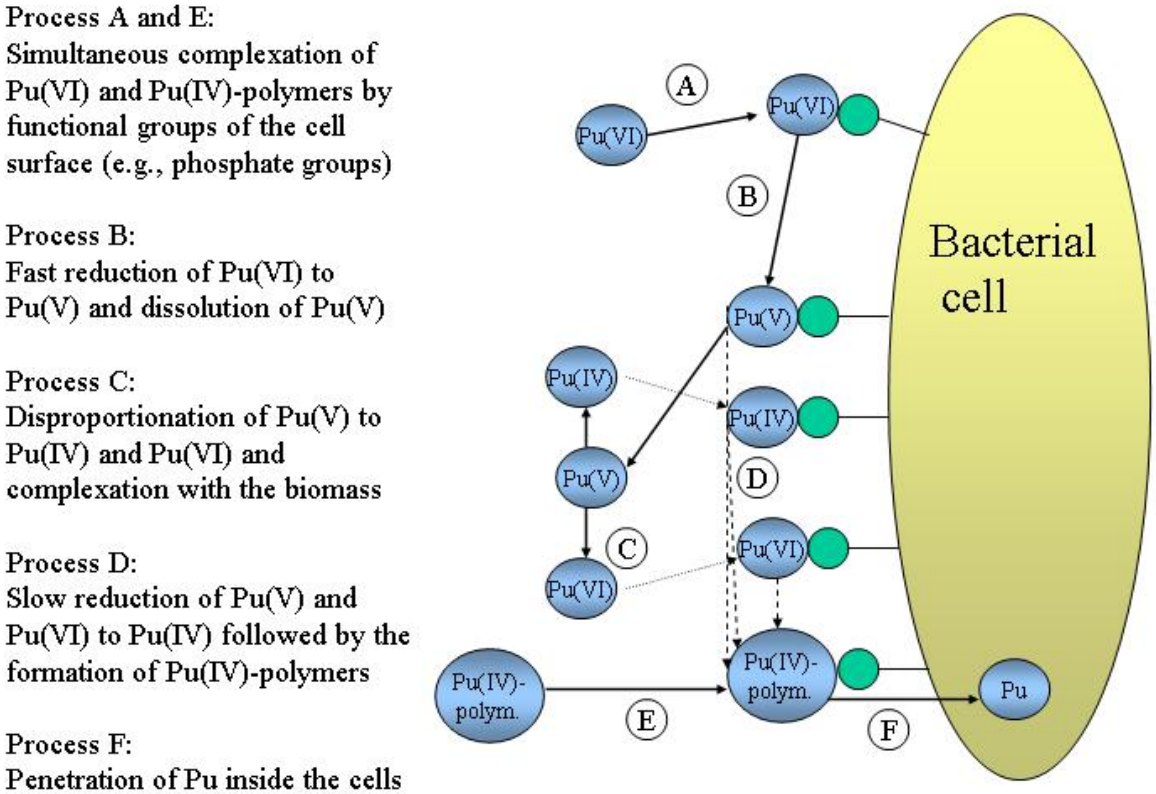

Fig. 3.4.12: Illustration of the different processes of the interaction of Pu with *D. äspöensis* based on the schema developed by Panak et al. in [55].

We could demonstrate that there is a strong interaction of the main Pu species, Pu(VI) and Pu(IV)-polymer, with cells of *D. äspöensis*. The interaction with plutonium includes six processes which have different time scales. In a first step, the Pu(VI) and Pu(IV)-polymers are bound to the biomass. The Pu(VI) is reduced to Pu(V) in a fast reaction due to the activity of

the cells. This process is almost finished after 24 h. We assume an enzymatic reduction reaction because we know from former investigations with uranium, that the majority of the cells should be metabolically active after 24 h (see chapter 3.1.3). As shown in Table 3.4.6, most of the formed Pu(V) dissolves due to the weak complexing properties. The dissolved Pu(V) disproportionates to Pu(IV) and Pu(VI). The measured amount of Pu(IV) and Pu(VI) associated with the biomass suggests an interaction of these species with functional groups (e.g., phosphate groups) of the cell surface structure. Imaginable would be also a subsequent slow reduction of the biosorpt Pu(V) and Pu(VI) to Pu(IV) followed by the formation of Pu(IV)-polymers. As already described for uranium (see chapters 3.1.3 and 3.1.5), we assume also for Pu the damage of the cell membranes due to the metal stress. Therefore, we conclude from the increased amount of Pu which is strongly bound a penetration of Pu species (e.g., Pu(IV)-polymers) inside the bacterial cell.

Our study has shown that the interaction of plutonium with the SRB *D. äspöensis* causes changes of the oxidation state of Pu which have an impact on the migration behavior. In contrast to the results of Panak et al. [55] with aerobic soil bacteria, where one third of the initial Pu(VI) was reduced to Pu(V) after 24 h, we observed that app. 98% of the Pu(VI) was reduced to Pu(V) in the same time range. The reduction of the Pu(VI) bound to the biomass to Pu(V) leads to an increased dissolution of the cell bound plutonium. On the other hand, we observed an immobilization of Pu(IV)-polymers by the bacteria.

4 Summary and conclusions

In order to improve the knowledge on microbial processes with actinides in different oxidation states, we investigated the interaction mechanisms of U(VI), Cm(III), Np(V), and Pu [Pu(VI), Pu(IV)-polymers] with the sulfate-reducing bacterial (SRB) strain *Desulfovibrio äspöensis*. Our Swedish partners could show that SRB are frequently occurring in the deep grantic aquifer system at the Äspö hard rock laboratory [1-3]. They could even identify a new SRB strain called *D. äspöensis* [4].
Before the present project, it was unknown in which way cells of *D. äspöensis* are interacting with the selected actinides.

The cells of *D. äspöensis* were successfully cultivated under anerobic conditions in liquid and on solid medium. The purity of the cultures was verified using light microscopy and by applying the molecular microbiological method ARDREA. Under the given experimental conditions, the cells reached the stationary phase of the growth curve after 8 to 9 days after inoculation at 22 °C.

In this project, we could demonstrate the removal of U(VI) due to the activity of the cells of *D. äspöensis* for the first time. Three parameters are influencing the removal efficiency of U(VI): a) the interaction time, b) the pH, and c) the initial uranium concentration, $[U]_{initial}$, present in the test solutions. The amount of U bound to the biomass increased with increasing pH from 3 to 6. However, at pH 8 a strong decrease of the amount of accumulated uranium was observed. The cells of *D. äspöensis* removed 55% of the U(VI), 10.1 $mg/g_{dry\ weight}$, from an aqueous solution of 14.6 mg/l U(VI), supplemented with 10 mM lactate, after 72 h of incubation at pH 5. Within this investigation the first direct spectroscopic proof for a reduction of U(VI) to U(IV) most likely by an enzymatic reaction due to the activity of the cells was obtained. The toxicity of U(VI) towards *D. äspöensis* could by proved using microbiological methods. As a consequence, the membrane system gets damaged and uranium can penetrate inside the bacterial cells. The results are indicating a complex interaction mechanism consisting of biosorption, bioreduction, and bioaccumulation.

Within this project, we could show the removal of Np(V) from the solution by cells of *D. äspöensis* for the first time. The cells of this bacterium removed only 2.5 % of the Np(V), 0.69 $mg/g_{dry\ weight}$, from an aqueous solution of 23.7 mg/l Np(V) under steady state conditions

at pH 5. Similar to U(VI), the interaction time, the pH, and the initial neptunium concentration, $[Np]_{initial}$, present in the test solutions are influencing the amount of bound Np(V) to the cells. The time dependent decrease of the Np concentration in solution shows slightly slower kinetics compared to uranium. Furthermore, Np(V) exhibits a weaker tendency to interact with the biomass than U(VI). Interestingly, no difference was detected in the amount of accumulated Np by the biomass in the presence or the absence of U in the test solutions. This might indicate the occurrence of different binding places and/or binding modes for Np and U on the cell envelope of *D. äspöensis*.

In the case of plutonium, we developed a model which describes the ongoing processes on the basis of our results and taking into the consideration the knowledge in the literature [55].
In a first step, the Pu(VI) and Pu(IV)-polymers are bound to the biomass. For instance, cells of *D. äspöensis* removed 30% of ^{242}Pu, 4.70 $mg/g_{dry\ weight}$, from an aqueous solution of 15.7 mg/l ^{242}Pu after 72 h of incubation at pH 5. The Pu(VI) is reduced to Pu(V) in a fast reaction due to the activity of the cells. Most of the formed Pu(V) dissolves due to the weak complexing properties. The dissolved Pu(V) disproportionates to Pu(IV) and Pu(VI). We found indications for an interaction of the disproportionation products with functional groups (e.g., phosphate groups) of the cell surface structure. The biosorpt Pu(V) and Pu(VI) could be transferred to Pu(IV) in a slow reaction, whereas the Pu(IV) probably forms Pu(IV)-polymers in a subsequent reaction. The experiments gave also evidence for a penetration of Pu species (e.g., Pu(IV)-polymers) inside the bacterial cell. Similar to U(VI) and Np(V), the interaction of Pu with *D. äspöensis* is a complex mechanism which consists of sub-processes.

For Cm(III) at a trace concentration level of $3x10^{-7}$ M, we interpret the pH dependence of the fluorescence emission spectra with a pure biosorption forming an inner-sphere surface complex of Cm(III) onto the *D. äspöensis* cell envelope. This Cm(III)-*D. äspöensis*-surface complex is characterized by its emission spectrum (peak maximum at 600.1 nm) and its fluorescence lifetime (162 ± 5 µs). From other investigations of biological systems and from a spectroscopic study of the complexation of Cm(III) with adenosine 5'-triphosphate, we conclude that mainly organic phosphate groups of the cell surface are involved in the bonding of Cm(III) to *D. äspöensis*. A reversible biosorption reaction was observed. Under the given experimental conditions, more than 80% of the Cm is bound to the bacteria at pH > 5.5. No evidence was found for an incorporation of Cm(III) into the bacterial cells at this low initial concentration (0.093 $mg/g_{dry\ weight}$).

Our study demonstrates that the interaction of uranium, plutonium and possibly neptunium with *D. äspöensis* causes changes of the oxidation state of the actinides which have an impact on the migration behavior. Assuming attached cells of *D. äspöensis* to the granitic rock of the Äspö HRL, released Cm(III) in the aquifer gets immobilized due to a biosorption on the bacterial cells in the neutral pH range. In the case of the other actinides, the interaction mechanism is more complex and consists of sub-processes. To summarize, the strength of the interaction of *D. äspöensis* with the selected actinides at pH 5 and actinide concentrations ≥ 10 mg/l ([Cm] 0.07 mg/l) follows the pattern: Cm > U > Pu >> Np.

The results of these studies improve the knowledge on direct interactions of cells of the type *Desulfovibrio äspöensis* with actinides. Important results were obtained about the cultivation and characterization of the biomass, their potential to remove the selected actinides from the surrounding solution and about the different interaction mechanisms dependent on the nature of the actinide element. Taking all results together they contribute to a more realistic description of the influence of microbial actions on the migration behavior of actinides in the environment and are helpful for an improved risk assessment for instance for potential underground nuclear waste repositories.

Further studies should focus on two main directions. The first one should be concentrated on direct interactions of actinides with recovered bacteria from potential nuclear waste repository areas (granitc rock: Äspö HRL, clay formation, salt). In a first step, the microbial diversity should be investigated to identify the dominating strains of bacteria. Which are then used to determine their interaction behavior with selected actinides. The second research objective is focused on the less studied indirect interaction path dealing with the mobilization of actinides by microbially produced bioligands for instance in the Äspö aquifer. One goal will be the determination of stability constants and the structure of the formed actinide-bioligand species. These constants will be used directly in risk assessment programs.
This strategy could help to identify the predominant interaction mechanisms between microbes and actinides.

5 References

[1] Pedersen, K.; Arlinger, J.; Ekendahl, S.; Hallbeck, L.: FEMS Microbiol. Ecol. **19**, 249 (1996).

[2] Kotelnikova, S.; Pedersen, K.: FEMS Microbiol. Ecol. **26**, 121 (1998).

[3] Pedersen, K.: Engineer. Geol. **52**, 163 (1999).

[4] Motamedi, M.; Pedersen, K.: Int. Syst. Bacteriol. **48**, 311 (1998).

[5] Selenska-Pobell, S.; Flemming, K.; Kampf, G.; Radeva, G.: Antonie van Leewenhuek **79**, 149 (2001).

[6] Bruynesteyn, A.: J. Biotechnol. **11**, 1 (1989).

[7] Hutchins, S. R.; Davidson, M. S.; Brierley, J. A.; Brierley, C. L.: Ann. Rev. Microbiol. **40**, 311 (1986).

[8] Rawling, D. E.; Silver, S.: Bio/Technol. **13**, 773 (1995).

[9] Lloyd, J. R.; Chesnes, J.; Glasauer, S.; Bunker, D. J.; Livens, F. R.; Lovley, D. R.: Geomicrobiol. **19**, 103 (2002).

[10] Francis, A. J.; Gillow, J. B.; Dodge, C. J.; Dunn, M.; Mantioue, K.; Streitelmeier, B. A.; Pansoy-Hejelik, M. E.; Papenguth, H. W.: Radiochim. Acta **82**, 347 (1998).

[11] Francis, A. J.: J. Alloys Comp. **271/273**, 78 (1998).

[12] Lovley, D. R.; Phillips, E. J. P.: Environ. Sci. Technol. **26**, 2228-2234 (1992).

[13] Lovley, D. R.; Roden, E. E.; Phillips, E. J. P.; Woodward, J. C.: Mar. Geol. **113**, 41 (1993).

[14] Lovley, D. R.; Phillips, E. J. P.: Appl. Environ. Microbiol. **58(3)**, 3572-3576 (1993).

[15] H. Moll, Merroun, M.; Stumpf, Th.; Geipel, G.; Selenska-Pobell, S.; Hennig, C.; Roßberg, A.; Bernhard, G.: *Interaction of Desulfovibrio äspöensis with Actinides*, presented at the 9th International Conference MIGRATION'03, Gyeongju, Korea, September 2003; Paper B4-4.

[16] Panak, P.; Hard, B. C.; Pietzsch, K.; Kutschke, S.; Röske, K.; Selenska-Pobell, S.; Bernhard, G.; Nitsche, H.: J. Alloys Comp. **271/273**, 262 (1998).

[17] Lovley, D. R.; Phillips, E. J. P.: Appl. Environ. Microbiol. **58**, 850 (1992).

[18] Alonso, J. L.; Mascellaro, S.; Moreno, Y.; Ferrús, M. A.; Hernández, J.: Appl. Environ. Microbiol. **68**, 5151-5154 (2002).

[19] Reich, T.; Bernhard, G.; Geipel, G.; Funke, H.; Hennig, C.; Roßberg, A.; Matz, W.; Schell, N.; Nitsche, H.: Radiochim. Acta **88**, 633 (2000).

[20] Koningsberger, D. C., Prins, R. (eds): X-ray Absorption: Principles, Application, Techniques of EXAFS, SEXAFS and XANES. Wiley, New York, USA, 1988.

[21] George, G. N.; Pickering, I. J.: EXAFSPAK: A Suite of Computer Programs for Analysis of X-ray Absorption Spectra. Stanford Synchrotron Radiation Laboratory, Stanford, USA, 1995.

[22] Zabinsky, S. I.; Rehr, J. J.; Ankudinov, A.; Albers, R. C.; Eller, M. J.: Phys. Rev. B, **52**, 2995 (1995).

[23] Roßberg, A.; Reich, T.; Bernhard, G.: Anal. Bioanal. Chem. **376**, 631 (2003).

[24] Beverige, T. J.; Koval, S. F.: Appl. Environ. Microbiol. **42**, 325 (1981).

[25] Merroun, M.; Hennig, C.; Rossberg, A.; Reich, T.; Selenska-Pobell, S.: Radiochim. Acta **91**, 583 (2003).

[26] Merroun, M.; Roßberg, A.; Hennig, C.; Reich, T.; Selenska-Pobell, S.: FZR Annual Report 2002, FZR-373 p. 33 (2003).

[27] Geipel, G.; Bernhard, G.; Brendler, V.; Nitsche, H.: Radiochim. Acta **82**, 59 (1998).

[28] Lloyed, J. R., Macaskie, L. E.: Biochemical basis of microbe-radionuclide interactions. In: *Interaction of Microorganisms with Radionuclides*. (Keith-Roach, M., Livens, F. eds.) Elsevier Sciences, Oxford (2000).

[29] Kim, J. I.; Klenze, R.; Wimmer, H.: Eur. J. Solid State Inorg. Chem. **28**, 347 (1991).

[30] Fanghänel, Th.; Kim, J. I.: J. Alloys Comp. **271/273**, 728 (1998).

[31] Klenze, R.; Kim, J. I.; Wimmer, H.: Radiochim. Acta **52/53**, 97 (1991).

[32] Panak, P.; Klenze, R.; Kim, J. I.: Radiochim. Acta **74**, 141 (1996).

[33] Kim, J. I.; Rhee, D. S.; Wimmer, H.; Buckau, G.; Klenze, R.: Radiochim. Acta **62**, 35 (1993).

[34] Kim, J. I.; Wimmer, H.; Klenze, R.: Radiochim. Acta **54**, 35 (1991).

[35] Moulin, C.; Decambox, P.; Mauchien, P.: Radiochim. Acta **52/53**, 119 (1991).

[36] Buckau, G.; Kim, J. I.; Klenze, R.; Rhee, D. S.; Wimmer, H.: Radiochim. Acta **57**, 105 (1992).

[37] Stumpf, Th.; Fanghänel, Th.; Grenthe, I.: J. Chem. Soc., Dalton Trans., 3799 (2002).

[38] Moll, H.; Geipel,G.; Bernhard, G.: Inorg. Chim. Acta, in press (2005).

[39] Chung, K. H.; Klenze, R.; Park, K. K.; Paviet-Hartmann, P.; Kim, J. I.: Radiochim. Acta **82**, 215 (1998).

[40] Stumpf, Th.; Rabung, Th.; Klenze, R.; Geckeis, H.; Kim, J. I.: J. Colloid Interface Sci. **238**, 219 (2001).

[41] Stumpf, Th.; Bauer, A.; Coppin, F.; Kim, J. I.: Environ. Sci. Technol. **35**, 3691 (2001).

[42] Tits, J.; Stumpf, Th.; Rabung, Th.; Wieland, E.; Fanghänel, Th.: Environ. Sci. Technol. **37**, 3568 (2003).

[43] Ozaki, T.; Gillow, J. B.; Francis, A. J.; Kimura, T.; Ohnuki, T.; Yoshida, Z.: J. Nucl. Sci. Technol. **3**, 950 (2002).

[44] Moll, H.; Stumpf, Th.; Merroun, M.; Roßberg, A.; Selenska-Pobell, S.; Bernhard, G.: Environ. Sci. Technol. **38**, 1455 (2004).

[45] Fanghänel, Th.; Kim, J. I.; Paviet, P.; Klenze, R.; Hauser, W.: Radiochim. Acta **66/67**, 81 (1994).

[46] Wimmer, H.; Klenze, R.; Kim, J. I.: Radiochim. Acta **56**, 79 (1992).

[47] Fanghänel, Th.; Kim, J. I.; Klenze, R.; Kato, J.: J. Alloys Comp. **225**, 308 (1995).

[48] Beitz, J. V.; Bowers, D. L.; Doxtader, M. M.; Maroni, V. A.; Reed, D. T.: Radiochim. Acta **44/45**, 87 (1988).

[49] Kimura, T.; Choppin, G. R.: J. Alloys Comp. **213/214**, 313 (1994).

[50] Carnall, W. T.; Crosswhite, H. M.: Report ANL-84-90 1995.

[51] Madigan, M. T.; Martinko, J. M.; Parcker, J. In: Brock Biology of Microorganisms, 9th ed.; Corey, P. F. Ed.; Prentice-Hall: Upper Saddle River, New Jersey, 2000; Chapter 3.

[52] Ferris, F. G.; Beverige, T. J.: FEMS Microbiol. Lett. **24**, 43 (1984).

[53] Merroun, M. L.; Selenska-Pobell, S.: BioMetals **14**, 171 (2001).

[54] Merroun, M. L.; Geipel, G.; Nicolai, R.; Heise, K.-H.; Selenska-Pobell, S.: BioMetals **16**, 331 (2003).

[55] Panak, P. J.; Nitsche, H.: Radiochim. Acta **89**, 499 (2001).

[56] Panak, P. J.; Raff, J.; Selenska-Pobell, S.; Geipel, G.; Bernhard, G., Nitsche, H.: Radiochim. Acta **88**, 71 (2000).

[57] Günther, A.; Bernhard, G.; Geipel, G.; Reich, T.; Roßberg, A.; Nitsche, H.: Radiochim. Acta **91**, 319 (2003).

[58] Shanbhag, S. M.; Choppin, G. R.: Inorg. Chim. Acta **139**, 119 (1987).

[59] Purves, W. K.; Sadava, D.; Orians, G. H.; Heller, H.C.: Life: The Science of Biology, Seventh Edition, Sinauer Associates, Inc. Publishers, Sunderland, MA, USA (2003).

[60] Rizkalla, E. N.; Nectoux, F.; Dabos-Seigon, S.; Pages, M.: Inorg. Biochem. 51, 701 (1993).

[61] Geipel, G.; Bernhard, G.; Brendler, V.; Reich, T.*: Complex formation between uranium(VI) and adenosine triphosphate*. Presented at the 5th International Conference on Nuclear and Radiochemistry NRC 5, Pontresina, Switzerland, September 2000; Extended Abstracts Volume 2, Pages 473-476.

[62] Binstead, R. A.; Zuberbühler, A. D.; Jung, B.: SPECFIT Global Analysis System Version 3.0.34 (2003).

[63] Oscarson, J. L.; Wang, P.; Gillespie, S. E.; Izatt, R. M.: J. Solution Chem. **24**, 171 (1995).

[64] Songkasiri, W.; Reed, D. T.; Rittmann, B. E.: Radiochim. Acta **90**, 785-789 (2002).

[65] Lloyd, J. R.; Yong, P.; Macaskie, L. E.: Environ. Sci. Technol. **34**, 1297-1301 (2000).

[66] Rittmann, B.E.; Banaszak, J. E.; Reed, D. T.: Biodegradation **13**, 329-342 (2002).

[67] Choppin, G.R.: Radiochim. Acta **43**, 82 (1988).

[68] Wildung, R. E., Garland, T. R.: *The relationship of microbial processes to the fate and behavior of transuranic elements in soils, plants, and animals.* In: *Transuranic elements in the environment.* (Hanson, W.C., Ed.), DOE/TIC-22800, Technical Information Center/US Department of Energy, Washington, DC (1980), p. 300.

[69] Francis, A. J.; Gillow, J. B.; Dodge, C. J.; Dunn, M.; Mantioue, K.; Streitelmeier, B. A.; Pansoy-Hejelik, M. E.; Papenguth, H. W.: Radiochim. Acta **82**, 347 (1998).

[70] Strietelmeier, B. A.; Sebring, R. J.; Gillow, J. B.; Dodge, C. J.; Pansoy-Hjelvik, M. E.; Kraus, S. M.; Leonard, P. A.; Triay, I. R.; Francis, A. J.; Papenguth, H. W.*: Plutonium interaction with a bacterial strain isolated from the waste isolation pilot plant (WIPP) environment.* American Chemical Society, Division of Environmental Chemistry Preprints of Extended Abstracts Vol. 36 (2) (1996).

[71] Rusin, P. A.; Quintana, L.; Brainard, J. R.; Strietelmeier, B. A.; Tait, C. D.; Ekberg, S.A.; Palmer, P. D.; Newton, T. W.; Clark, D. L.: Environ. Sci. Technol. **28**, 1686 (1994).

[72] John, S. G.; Ruggiero, C. E.; Hersman, L. E.; Tung, C.-S.; Neu, M. P.: Environ. Sci. Technol. **35**, 2942 (2001).

[73] Keller, C.: *The Chemistry of the Transuranium Elements*, Volume 3, Verlag Chemie GmbH, Weinheim, Germany (1971).

[74] Nitsche, H.; Lee, S. C.; Gatti, R. C.: J. Radioanal. Nucl. Chem. Articles **124/1**, 171-185 (1988).

[75] Nitsche, H.; Roberts, K.; Xi, R.; Prussin, T.; Becraft, K.; Mahamid, A. I.; Silber, H. S.; Carpenter, S. A.; Gatti, R. C.: Radiochim. Acta **66/67**, 3-8 (1994).

[76] Eberle, S. H., Schaefer, J. B.: Inorg. Nucl. Chem. Letters **4**, 283-287 (1968).

[77] Magon, L., Tomat, G., Bismondo, A., Portanova, R., Croatto, U.: Gazetta Chimica Italiana **104**, 967-976 (1974).

[78] Moll, H.; Geipel, G.; Reich, T.; Bernhard, G.; Fanghänel, Th.; Grenthe, I.: Radiochim. Acta **91**, 11-20 (2003).

[79] Fuger, J.; Nitsche, H.; Potter, P.; Rand, M. H.; Rydberg, J.; Spahiu, K.; Sullivan, J. C.; Ullman, W.; Vitorge, P.; Wanner, H.; Lemire R. J.: *Chemical Thermodynamics 4 of Neptunium and Plutonium*, NEA OECD, Issy-les-Moulineaux, France (2001).

6 Acknowledgement

The authors are indebted for the use of the Cm-248 to the U.S. Department of Energy, Office of Basic Energy Sciences, through the transplutonium element production facilities at Oak Ridge National Laboratory which was made available as part of a collaboration between FZR and the Lawrence Berkeley National Laboratory (LBNL).

We thank U. Schaefer for the ICP-MS measurements and C. Nebelung for her help in performing the LSC measurements. Thanks are given to S. Matys and M. Maitz for valuable help and support during the live/dead investigations with flow cytometry and fluorescence microscopy. The authors would like to thank K. Flemming and J. Raff for their technical assistance in all microbiology questions.

The TEM/EDX measurements were performed at the University of Granada (Spain). In particular, thanks are given to M. del Mar Abad Ortega, C. Hidalgo Sanchez and M.T. González-Muñoz for their support and help during the measurements.

The XAS measurements were performed at BM20 (ROBL) at the European Synchrotron Radiation Facility (ESRF) in Grenoble (France). In particular, thanks are given to T. Reich, C. Hennig, H. Funke, M. Walter for their support during the XAS measurements and their help in evaluating the data.

The authors would like to thank K. Pedersen and his group at the Göteborg University, Department of Cell and Molecular Biology (Sweden) for the fruitful discussions and helpful comments concerning the cultivation of *D. äspöensis*.

At this place we would like to take the opportunity to thank all colleagues who contributed to the success of this work.